Conclusions

We proposed a mechanism of resistance against NFV due to the nonactive site mutation N88S in CRF01_AE PR through computational simulations. CRF01_AE PR has polymorphisms at nonactive sites, unlike subtype B PR. Nevertheless, the polymorphisms affect the binding affinities between NFV and PR variants that have the D30N or N88S mutation. The simulations suggest that N88S in CRF01_AE PR confers NFV resistance by reducing interaction energy between D30 and NFV. N88S creates hydrogen bonds between the D30 and S88 side chains and causes conformational changes at D30. These changes reduce the interactions between D30 and NFV. Furthermore, we proposed an explanation of why the emergence rates of D30N and N88S differ between subtypes B and AE HIV-1. The M36I mutation seen in the natural polymorphisms of CRF01_AE PR is particularly involved in the difference in the emergence rates of D30N and N88S.

Experimental Section

Force Field Parameters. Before carrying out molecular dynamics (MD) simulations, we improved the torsional force field parameters for benzamide and determined the restrained electrostatic potential (RESP)[51] charges for NFV. The improved torsional parameters were generated in the same manner as that for the development of the AMBER ff03 force field.[43] First, RESP charges of benzamide were determined on the basis of data from quantum chemical calculations. Geometric optimization was performed at the HF/6-31G(d,p) level, and the electrostatic potential was calculated at the B3LYP/cc-pVTZ level under solvation conditions with ether ($\epsilon = 4$) by the IEFPCM method using the Gaussian 03 program.[52] The partial atom charges were determined using the RESP method so that the atom charges could reproduce the values of the calculated electrostatic potential at the surrounding points of the benzamide. Charges were equalized between two atoms if they were the same element and had the same bond coordination. Second, a potential energy curve was obtained by repeating the energy calculations with 5° stepwise changes in the torsional angle around the torsional axis. Energy calculations were executed at the MP2/cc-pVTZ level in the ether phase after geometric optimizations at the HF/6-31G(d,p) level. Third, the torsional parameters were obtained by fitting them to the potential energies from quantum chemical calculations. The torsional parameter for CA−CA−C−N was assumed to be equal to that for CA−CA−C−O. RESP charges for NFV were also determined in the same manner as that described above.

Molecular Dynamics (MD) Simulations. Minimizations and MD simulations were carried out using the Sander module of AMBER 8.[53] The AMBER ff03 force field[43] was used as the parameters for proteins, ions, and water molecules. The general AMBER force field[44] and our developed force field were used as the parameters for NFV.

We examined the structure of each of the six PRs in complex with NFV: wild-type (WT) PR, D30N PR, and N88S PR of subtype B HIV-1 (labeled B(WT), B(D30N), and B(N88S), respectively); the reference (Ref) PR, D30N PR, N88S PR of subtype AE HIV-1 in complex with NFV (AE(Ref), AE(D30N), and AE(N88S)). Additionally, we investigated the structures of M36I PR, M36I/N88S PR, and L10F/M36I/N88S PR of subtype B HIV-1 in complex with NFV (labeled B(M36I), B(M36I/N88S), and B(L10F/M36I/N88S), respectively). We used HXB2 as the WT sequence of subtype B HIV-1 and used NH1 as the reference sequence of subtype AE HIV-1.[54] Each initial structure for the PR in complex with NFV was modeled from the atom coordinates of an X-ray crystal structure (PDB code 1OHR)[42] using the LEaP module. Each model was placed in a rectangular box filled with about 8000 TIP3P water molecules,[55] with all of the crystal water molecules remaining. The cutoff distance for the long-range electrostatic and the van der Waals energy terms was set to 12.0 Å. The expansion and shrinkage of all covalent bonds connecting to hydrogen atoms were constrained using the SHAKE algorithm.[56] Periodic boundary conditions were applied to avoid the edge effect in all calculations. Energy minimization was achieved in three steps. First, movement was allowed only for water molecules and ions. Next, the ligand and the mutated residues were allowed to move in addition to the water molecules and ions. Finally, all atoms were permitted to move freely. In each step, energy minimization was executed by the steepest descent method for the first 10 000 steps and the conjugated gradient method for the subsequent 10 000 steps. After a 0.1 ns heating calculation until 310 K using the NVT ensemble, a 3.0 ns equilibrating calculation was executed at 1 atm and at 310 K using the NPT ensemble, with an integration time step of 2.0 fs. In the present calculations, the MD simulations showed no large fluctuations after about 2.0 ns of equilibrating calculations (Supporting Information Figures S8 and S9). Hence, atom coordinates were collected at an interval of 1.0 ps for the last 1.0 ns to analyze the structure in detail.

The protonation states of catalytic aspartates D25 and D25′ vary depending on the binding ligands or PRs.[57] Hence, the appropriate protonation states of catalytic aspartates should be determined for each model. Because NFV mimics a transition state of catalytic reaction by HIV-1 PR, we considered two kinds of protonation states.[58−60] One represented a combination of protonated D25 and unprotonated D25′ states, and the other represented the opposite combination. In order to determine the protonation states when NFV binds to each PR, the free energies of these two kinds of protonation states were compared using the calculation data obtained during 2.0−3.0 ns of MD simulations. The free energies were calculated on the basis of the MM/PBSA method.[61,62] We used the same parameter set for electrostatic and van der Waals energy terms as that used in the MD simulations, and no cutoff was applied for the calculation. Since the dielectric constants for the interior of proteins are considered to be in the range of 2−4, the interior dielectric constant was set to 2.0.[63] The outer dielectric constant was set to 80.0. The PBSA program was used to solve the Poisson−Boltzmann (PB) equation. B(D30N), B(M36I), B(L10F/M36I/N88S), and AE(D30N) were found to prefer the combination of protonated D25 and unprotonated D25′. The other five PRs (B(WT), B(N88S), B(M36I/N88S), AE(Ref), and AE(N88S)) preferred the combination of unprotonated D25 and protonated D25′ (Supporting Information Table S4).

Hydrogen Bond Criteria. The formation of a hydrogen bond was defined in terms of distance and orientation. The combination of donor D, hydrogen H, and acceptor A atoms with a D−H···A configuration was regarded as containing a hydrogen bond when the distance between donor D and acceptor A was shorter than 3.5 Å and the angle H−D−A was smaller than 60.0°.

Binding Free Energy Calculation. The binding free energy[64] was calculated by the following equation:

$$\Delta G_b = \Delta G_{int}^{ele} + \Delta G_{int}^{vdw} + \Delta G_{sol} - T\Delta S$$

where ΔG_b is the binding free energy in solution, ΔG_{int}^{ele} and ΔG_{int}^{vdw} are electrostatic and van der Waals interaction energies between a ligand and a protein, ΔG_{sol} is the solvation energy, and $-T\Delta S$ is the contribution of conformational entropy to the binding. In this study, assuming that the contribution of conformational entropy to the change in ΔG_b is negligible among mutants,[65] we neglected the entropy term in the energy estimation. ΔG_{int}^{ele} and ΔG_{int}^{vdw} were computed using the same parameter set as that used in the MD simulation, and no cutoff was applied to the calculation. Solvation energy ΔG_{sol} was calculated using the PBSA program. The interior dielectric constant was set to 2.0, and the outer dielectric constant was set to 80.0.[63] Furthermore, the contribution of each residue to the binding free energy was calculated. The total binding free energy was decomposed into the contribution from each individual residue by the MM/GBSA method. The modified GB model developed by Onufriev, Bashford, and Case[66] was used to calculate the solvation energy term. To ascertain whether or not

the MM/GBSA results were consistent with the MM/PBSA results, we compared the total binding free energy obtained by the MM/PBSA method with that obtained by the MM/GBSA method for all coordinates acquired through the MD simulation. The MM/GBSA results were confirmed to be highly correlated with the MM/PBSA results (correlation coefficient $r \geq 0.998$) (Supporting Information Figure S10).

Acknowledgment. This work was supported by a Health and Labor Science Research Grant for Research on HIV/AIDS from the Ministry of Health and Labor of Japan, by JSPS Research Fellowships for Young Scientists, and by a Grant-in-Aid for JSPS Fellows. A part of this work was also supported by a grant from the Japan Science and Technology Agency.

Supporting Information Available: A list of hydrogen bond networks in each model, determination of protonation states of catalytic aspartates, parameter development for the torsional parameters CA−CA−C−N and CA−CA−C−O, 3D plot of rmsd of the average structure from that of B(WT), contributions of each individual residue to the binding energy, rmsd plots during MD simulations, and results of principal component analyses. This material is available free of charge via the Internet at http://pubs.acs.org.

References

(1) Krausslich, H. G.; Wimmer, E. Viral proteinases. *Annu. Rev. Biochem.* **1988**, *57*, 701−754.
(2) Kohl, N. E.; Emini, E. A.; Schleif, W. A.; Davis, L. J.; Heimbach, J. C.; Dixon, R. A.; Scolinick, E. M.; Sigal, I. S. Active human immunodeficiency virus protease is required for viral infectivity. *Proc. Natl. Acad. Sci. U.S.A.* **1988**, *85*, 4686−4690.
(3) Craig, J. C.; Duncan, I. B.; Hockley, D.; Grief, C.; Roberts, N. A.; Mills, J. S. Antiviral properties of Ro 31-8959, an inhibitor of human immunodeficiency virus (HIV) proteinase. *Antiviral Res.* **1991**, *16*, 295−305.
(4) Vacca, J. P.; Dorsey, B. D.; Schleif, W. A.; Leven, R. B.; McDaniel, S. L.; Darke, P. L.; Zugay, J.; Quintero, J. C.; Blahy, O. M.; Roth, E.; Sardana, V. V.; Schlabach, A. J.; Graham, P. I.; Condra, J. H.; Gotlib, L.; Holloway, M. K.; Lin, J.; Chen, L.-W.; Vastag, K.; Ostvic, D.; Anderson, P. S.; Emini, E. A.; Huff, J. R. L-735,524: an orally bioavailable human immunodeficiency virus type 1 protease inhibitor. *Proc. Natl. Acad. Sci. U.S.A.* **1994**, *91*, 4096−4100.
(5) Kempf, D. J.; Marsh, K. C.; Denissen, J. F.; McDonald, E.; Vasavanonda, S.; Flentga, C. A.; Green, B. E.; Fino, L.; Park, C. H.; Kong, X.; Wideburg, N. E.; Saldivar, A.; Ruiz, L.; Kati, W. M.; Sham, H. L.; Robins, T.; Stewart, K. D.; Hsu, A.; Plattner, J. J.; Leonard, J. M.; Norbeck, D. W. ABT-538 is a potent inhibitor of human immunodeficiency virus protease and has high oral bioavailability in humans. *Proc. Natl. Acad. Sci. U.S.A.* **1995**, *92*, 2484−2488.
(6) Livington, D. J.; Pazhanisamy, S.; Porter, D. J.; Partaledis, J. A.; Tung, R. D.; Painter, G. R. Weak binding of VX-478 to human plasma proteins and implications for anti-human immunodeficiency virus therapy. *J. Infect. Dis.* **1995**, *172*, 1238−1245.
(7) Patick, A. K.; Mo, H.; Markowitz, M.; Appelt, K.; Wu, B.; Musick, L.; Kalish, V.; Kaldor, S.; Reich, S.; Ho, D.; Webber, S. Antiviral and resistance studies of AG1343, an orally bioavailable inhibitor of human immunodeficiency virus protease. *Antimicrob. Agents Chemother.* **1996**, *40*, 292−297 (Erratum, p 1575).
(8) Carrillo, A.; Stewart, K. D.; Sham, H. L.; Norbeck, D. W.; Kohlbrenner, W. E.; Leonard, J. M.; Kempf, D. J.; Molla, A. J. In vitro selection and characterization of human immunodeficiency virus type 1 variants with increased resistance to ABT-378, a novel protease inhibitor. *J. Virol.* **1998**, *72*, 7532−7541.
(9) Robinson, B. S.; Riccardi, K. A.; Gong, Y. F.; Guo, Q.; Stock, D. A.; Blair, W. S.; Terry, B. J.; Deminie, C. A.; Djang, F.; Colonno, R. J.; Lin, P. F. BMS-232632, a highly potent human immunodeficiency virus protease inhibitor that can be used in combination with other available antiretroviral agents. *Antimicrob. Agents Chemother.* **2000**, *44*, 2093−2099.
(10) Larder, B. A.; Hertogs, K.; Bloor, S.; van den Eynde, C.; DeCian, W.; Wang, Y.; Freimuth, W. W.; Tarpley, G. Tipranavir inhibits broadly protease inhibitor-resistant HIV-1 clinical samples. *AIDS* **2000**, *14*, 1943−1948.
(11) Koh, Y.; Nakata, H.; Maeda, K.; Ogata, H.; Bilcer, G.; Devasamudram, T.; Kincaid, J. F.; Boross, P.; Wang, Y. F.; Tie, Y.; Volarath, P.; Gaddis, L.; Harrison, R. W.; Weber, I. T.; Ghosh, A. K.; Mitsuya, H. Novel bis-tetrahydrofuranylurethane-containing nonpeptidic protease inhibitor (PI) UIC-94017 (TMC114) with potent activity against multi-PI-resistant human immunodeficiency virus in vitro. *Antimicrob. Agents Chemother.* **2003**, *47*, 3123−3129.
(12) Cornelissen, M.; van den Burg, R.; Zorgdrager, F.; Lukashov, V.; Goudsmit, J. pol gene diversity of five human immunodeficiency virus type 1 subtypes: evidence for naturally occurring mutations that contribute to drug resistance, limited recombination patterns, and common ancestry for subtypes B and D. *J. Virol.* **1997**, *71*, 6348−6358.
(13) Pieniazek, D.; Rayfield, M.; Hu, D. J.; Nkengasong, J.; Wiktor, S. Z.; Downing, R.; Biryahwaho, B.; Mastro, T.; Tanuri, A.; Soriano, V.; Lal, R.; Dondero, T. Protease sequences from HIV-1 group M subtypes A−H reveal distinct amino acid mutation patterns associated with protease resistance in protease inhibitor-naive individuals worldwide. HIV Variant Working Group. *AIDS* **2000**, *14*, 1489−1495.
(14) Vergne, L.; Peeters, M.; Mpoudi-Ngole, E.; Bourgeois, A.; Liegeois, F.; Toure-Kane, C.; Mboup, S.; Mulanga-Kabeya, C.; Saman, E.; Jourdan, J.; Reynes, J.; Delaporte, E. Genetic diversity of protease and reverse transcriptase sequences in non-subtype-B human immunodeficiency virus type 1 strains: evidence of many minor drug resistance mutations in treatment-naive patients. *J. Clin. Microbiol.* **2000**, *38*, 3919−3925.
(15) Grossman, Z.; Vardinon, N.; Chemtob, D.; Alkan, M. L.; Bentwich, Z.; Burke, M.; Gottesman, G.; Istomin, V.; Levi, I.; Maayan, S.; Shahar, E.; Schapiro, J. M. Genotypic variation of HIV-1 reverse transcriptase and protease: comparative analysis of clade C and clade B. *AIDS* **2001**, *15*, 1453−1460 (Erratum, p 2209).
(16) Ariyoshi, K.; Matsuda, M.; Miura, H.; Tateishi, S.; Yamada, K.; Sugiura, W. Patterns of point mutations associated with antiretroviral drug treatment failure in CRF01_AE (subtype E) infection differ from subtype B infection. *JAIDS, J. Acquired Immune Defic. Syndr.* **2003**, *33*, 336−342.
(17) Clemente, J. C.; Coman, R. M.; Thiaville, M. M.; Janka, L. K.; Jeung, J. A.; Nukoolkarn, S.; Govindasamy, L.: Agbandje-McKenna, M.; McKenna, R.; Leelamanit, W.; Goodenow, M. M.; Dunn, B. M. Analysis of HIV-1 CRF_01 A/E protease inhibitor resistance: structural determinants for maintaining sensitivity and developing resistance to atazanavir. *Biochemistry* **2006**, *45*, 5468−5477.
(18) Patick, A. K.; Duran, M.; Cao, Y.; Shugarts, D.; Keller, M. R.; Mazabel, E.; Knowles, M.; Chapman, S.; Kuritzkes, D. R.; Markowitz, M. Genotypic and phenotypic characterization of human immunodeficiency virus type 1 variants isolated from patients treated with the protease inhibitor nelfinavir. *Antimicrob. Agents Chemother.* **1998**, *42*, 2637−2644.
(19) Ziermann, E.; Limoli, K.; Das, K.; Arnold, E.; Petropoulos, C. J.; Parkin, N. T. A mutation in human immunodeficiency virus type 1 protease, N88S, that causes in vitro hypersensitivity to amprenavir. *J. Virol.* **2000**, *74*, 4414−4419.
(20) Sugiura, W.; Matsuda, Z.; Yokomaku, Y.; Hertogs, K.; Larder, B.; Oishi, T.; Okano, A.; Shiino, T.; Tatsumi, M.; Matsuda, M.; Abumi, H.; Takata, N.; Shirahata, S.; Yamada, K.; Yoshikura, H.; Nagai, Y. Interference between D30N and L90M in selection and development of protease inhibitor-resistant human immunodeficiency virus type 1. *Antimicrob. Agents Chemother.* **2002**, *46*, 708−715.
(21) Resch, W.; Ziermann, R.; Parkin, N.; Gamarnik, A.; Swanstrom, R. Nelfinavir-resistant, amprenavir-hypersusceptible strains of human immunodeficiency virus type 1 carrying an N88S mutation in protease have reduced infectivity, reduced replication capacity, and reduced fitness and process the Gag polyprotein precursor aberrantly. *J. Virol.* **2002**, *76*, 8659−8666.
(22) Ode, H.; Ota, M.; Neya, S.; Hata, M.; Sugiura, W.; Hoshino, T. Resistant mechanism against nelfinavir of human immunodeficiency virus type-1 proteases. *J. Phys. Chem. B* **2005**, *109*, 565−574.
(23) Mahalingam, B.; Louis, J. M.; Reed, C. C.; Adomat, J. M.; Krouse, J.; Wang, Y.-F.; Harrison, R. W.; Weber, I. T. Structural and kinetic analysis of drug resistant mutants of HIV-1 protease. *Eur. J. Biochem.* **1999**, *263*, 238−245.
(24) Hong, L.; Zhang, X. C.; Hartsuck, J. A.; Tang, J. Crystal structure of an in vivo HIV-1 protease mutant in complex with saquinavir: insights into the mechanisms of drug resistance. *Protein Sci.* **2000**, *9*, 1898−1904.
(25) Mahalingam, B.; Louis, J. M.; Hung, J.; Harrison, R. W.; Weber, I. T. Structural implications of drug-resistant mutants of HIV-1 protease: high-resolution crystal structures of the mutant protease/substrate analogue complexes. *Proteins: Struct., Funct., Genet.* **2001**, *43*, 455−464.
(26) Mahalingam, B.; Boross, P.; Wang, Y.-F.; Louis, J. M.; Fischer, C. C.; Tozser, J.; Harrison, R. W.; Weber, I. T. Combining mutations in HIV-1 protease to understand mechanisms of resistance. *Proteins: Struct., Funct., Genet.* **2002**, *48*, 107−116.

(27) Weber, J.; Mesters, J. R.; Lepsik, M.; Prejdova, J.; Svec, M.; Sponarova, J.; Mlcochova, P.; Skalika, K.; Strisovsky, K.; Uhlikova, T.; Soucek, M.; Machala, L.; Stankova, M.; Vondrasek, J.; Klimkait, T.; Kraeusslich, H.-G.; Hilgenfeld, R.; Konvalinka, J. Unusual binding mode of an HIV-1 protease inhibitor explains its potency against multi-drug-resistant virus strains. *J. Mol. Biol.* **2002**, *324*, 739−754.

(28) King, N. M.; Melnick, L.; Prabu-Jeyabalan, M.; Nalivaika, E. A.; Yang, S. S.; Gao, Y.; Nie, X.; Zepp, C.; Heefner, D. L.; Schiffer, C. A. Lack of synergy for inhibitors targeting a multi-drug-resistant HIV-1 protease. *Protein Sci.* **2002**, *11*, 418−429.

(29) Prabu-Jeyabalan, M.; Nalivaika, E. A.; King, N. M.; Schiffer, C. A. Viability of a drug-resistant human immunodeficiency virus type 1 protease variant: structural insights for better antiviral therapy. *J. Virol.* **2003**, *77*, 1306−1315.

(30) Mahalingam, B.; Wang, Y.-F.; Boross, P. L.; Tozser, J.; Louis, J. M.; Harrison, R. W.; Weber, I. T. Crystal structures of HIV protease V82A and L90M mutants reveal changes in the indinavir-binding site. *Eur. J. Biochem.* **2004**, *271*, 1516−1524.

(31) King, N. M.; Prabu-Jeyabalan, M.; Nalivaika, E. A.; Wigerinck, P.; Béthune, M. P.; Schiffer, C. A. Structural and thermodynamic basis for the binding of TMC114, a next-generation human immunodeficiency virus type 1 protease inhibitor. *J. Virol.* **2004**, *78*, 12012−12021.

(32) Prabu-Jeyabalan, M.; Nalivaika, E. A.; King, N. M.; Schiffer, C. A. Structural basis for coevolution of a human immunodeficiency virus type 1 nucleocapsid-p1 cleavage site with a V82A drug-resistant mutation in viral protease. *J. Virol.* **2004**, *78*, 12446−12454.

(33) Skalova, T.; Dohnalek, J.; Duskova, J.; Petrokova, H.; Hradilek, M.; Soucek, M.; Konvalinka, J.; Hasek, J. HIV-1 protease mutations and inhibitor modifications monitored on a series of complexes. Structural basis for the effect of the A71V mutation on the active site. *J. Med. Chem.* **2006**, *49*, 5777−5784.

(34) Rick, S. W.; Topol, I. A.; Erickson, J. W.; Burt, S. K. Molecular mechanisms of resistance: free energy calculations of mutation effects on inhibitor binding to HIV-1 protease. *Protein Sci.* **1998**, *8*, 1750−1756.

(35) Piana, S.; Carloni, P.; Rothlisberger, U. Drug resistance in HIV-1 protease: Flexibility-assisted mechanism of compensatory mutations. *Protein Sci.* **2002**, *11*, 2393−2402.

(36) Clemente, J. C.; Hermrajani, R.; Blum, L. E.; Goodenow, M. M.; Dunn, B. M. Secondary mutations M36I and A71V in the human immunodeficiency virus type 1 protease can provide an advantage for the emergence of the primary mutation D30N. *Biochemistry* **2003**, *42*, 15029−15035.

(37) Perryman, A. L.; Lin, J.-H.; McCammon, J. A. HIV-1 protease molecular dynamics of a wild-type and of the V82F/I84V mutant: possible contributions to drug resistance and a potential new target site for drugs. *Protein Sci.* **2004**, *13*, 1108−1123 (Erratum, p 1434).

(38) Wittayanarakul, K.; Aruksakunwong, O.; Saen-oon, S.; Chantratita, W.; Parasuk, V.; Sompornpisut, P.; Hannongbua, S. Insights into saquinavir resistance in the G48V HIV-1 protease: quantum calculations and molecular dynamic simulations. *Biophys. J.* **2005**, *88*, 867−879.

(39) Ode, H.; Neya, S.; Hata, M.; Sugiura, W.; Hoshino, T. Computational simulations of HIV-1 proteases−Multi-drug resistance due to non-active site mutation L90M. *J. Am. Chem. Soc.* **2006**, *128*, 7887−7895.

(40) Meiselbach, H.; Horn, A. H. C.; Harrer, T.; Sticht, H. Insights into amprenavir resistance in E35D HIV-1 protease mutation from molecular dynamics and binding free-energy calculations. *J. Mol. Model.* **2006**, *13*, 297−304.

(41) Batista, P. R.; Wilter, A.; Durham, E. H.; Pascutti, P. G. Molecular dynamics simulations applied to the study of subtypes of HIV-1 protease common to Brazil, Africa, and Asia. *Cell Biochem. Biophys.* **2006**, *44*, 395−404.

(42) Kaldor, S. W.; Kalish, V. J.; Davies, J. F.; Shetty, B. V.; Fritz, J. E.; Appelt, K.; Burgess, J. A.; Campanale, K. M.; Chirgadze, N. Y.; Clawson, D. K.; Dressman, B. A.; Hatch, S. D.; Khalil, D. A.; Kosa, M. B.; Lubbehusen, P. P.; Muesing, M. A.; Patick, A. K.; Reich, S. H.; Su, K. S.; Tatlock, J. H. Viracept (nelfinavir mesylate, AG1343): a potent, orally bioavailable inhibitor of HIV-1 protease. *J. Med. Chem.* **1997**, *40*, 3979−3985.

(43) Duan, Y.; Wu, C.; Chowdhury, S.; Lee, M. C.; Xiong, G.; Zhang, W.; Yang, R.; Cieplak, P.; Luo, R.; Lee, T. A point-charge force field for molecular mechanics simulations of proteins based on condensed-phase quantum mechanical calculations. *J. Comput. Chem.* **2003**, *24*, 1999−2012.

(44) Wang, J.; Wolf, R. M.; Cladwell, J. W.; Kollman, P. A.; Case, D. A. Development and testing of a general amber force field. *J. Comput. Chem.* **2004**, *25*, 1157−1174.

(45) http://structbio.vanderbilt.edu/archives/amber-archive/2003/0305.php.

(46) Johnson, V. A.; Brun-Vézinet, F.; Clotet, B.; Kuritzkes, D. R.; Pillay, D.; Schapiro, J. M.; Richman, D. D. Update of the drug resistance mutations in HIV-1: fall 2006. *Top. HIV Med.* **2006**, *14*, 125−130.

(47) Velazques-Campoy, A.; Todd, M. T.; Vega, S.; Freire, E. Catalytic efficiency and vitality of HIV-1 proteases from African viral subtypes. *Proc. Natl. Acad. Sci. U.S.A.* **2001**, *98*, 6062−6067.

(48) Velazques-Campoy, A.; Vega, S.; Fleming, E.; Bacha, U.; Sayed, Y.; Dirr, H. W.; Freire, E. Protease inhibition in African subtypes of HIV-1. *AIDS Rev.* **2003**, *5*, 165−171.

(49) Ohtaka, H.; Schön, A.; Freire, E. Multidrug resistance to HIV-1 protease inhibition requires cooperative coupling between distal mutations. *Biochemistry* **2003**, *42*, 13659−13666.

(50) Clemente, J. C.; Moose, R. E.; Hemrajani, R.; Whitford, L. R. S.; Govindasamy, L.; Rutzel, R.; McKenna, R.; Agbandje-McKenna, M.; Goodenow, M. M.; Dunn, B. M. Comparing the accumulation of active- and nonactive-site mutations in the HIV-1 protease. *Biochemistry* **2004**, *43*, 12141−12151.

(51) Cieplak, P.; Cornell, W. D.; Bayly, C.; Kollman, P. A. Application of the multimolecule and multiconformational RESP methodology to biopolymers: charge derivation for DNA, RNA, and proteins. *J. Comput. Chem.* **1995**, *16*, 1357−1377.

(52) Frisch, M. J.; Trucks, G. W.; Schlegel, H. B.; Scuseria, G. E.; Robb, M. A.; Cheeseman, J. R.; Montgomery, J. A., Jr.; Vreven, T.; Kudin, K. N.; Burant, J. C.; Millam, J. M.; Iyengar, S. S.; Tomasi, J.; Barone, V.; Mennucci, B.; Cossi, M.; Scalmani, G.; Rega, N.; Petersson, G. A.; Nakatsuji, H.; Hada, M.; Ehara, M.; Toyota, K.; Fukuda, R.; Hasegawa, J.; Ishida, M.; Nakajima, T.; Honda, Y.; Kitao, O.; Nakai, H.; Klene, M.; Li, X.; Knox, J. E.; Hratchian, H. P.; Cross, J. B.; Bakken, V.; Adamo, C.; Jaramillo, J.; Gomperts, R.; Stratmann, R. E.; Yazyev, O.; Austin, A. J.; Cammi, R.; Pomelli, C.; Ochterski, J. W.; Ayala, P. Y.; Morokuma, K.; Voth, G. A.; Salvador, P.; Dannenberg, J. J.; Zakrzewski, V. G.; Dapprich, S.; Daniels, A. D.; Strain, M. C.; Farkas, O.; Malick, D. K.; Rabuck, A. D.; Raghavachari, K.; Foresman, J. B.; Ortiz, J. V.; Cui, Q.; Baboul, A. G.; Clifford, S.; Cioslowski, J.; Stefanov, B. B.; Liu, G.; Liashenko, A.; Piskorz, P.; Komaromi, I.; Martin, R. L.; Fox, D. J.; Keith, T.; Al-Laham, M. A.; Peng, C. Y.; Nanayakkara, A.; Challacombe, M.; Gill, P. M. W.; Johnson, B.; Chen, W.; Wong, M. W.; Gonzalez, C.; Pople, J. A. *Gaussian 03*; Gaussian, Inc.: Wallingford, CT, 2004

(53) Case, D. A.; Darden, T. A.; Cheatham, T. E., III; Simmerling, C. L.; Wang, J.; Duke, R. E.; Luo, R.; Merz, K. M.; Wang, B.; Pearlman, D. A.; Crowley, M.; Brozell, S.; Tsui, V.; Gohlke, H.; Mongan, J.; Hornak, V.; Cui, G.; Beroza, P.; Schafmeister, C.; Caldwell, J. W.; Ross, W. S.; Kollman, P. A. *AMBER 8*; University of California: San Francisco, CA, 2004.

(54) Sato, H.; Shiino, T.; Kodaka, N.; Taniguchi, K.; Tomita, Y.; Kato, K.; Miyakuni, T.; Takebe, Y. Evolution and biological characterization of human immunodeficiency virus type 1 subtype E gp120 V3 sequences following horizontal and vertical virus transmission in a single family. *J. Virol.* **1999**, *73*, 3551−3559.

(55) Jorgensen, W. L.; Chandrasekhar, J.; Madura, J. D.; Impey, R. W.; Klein, M. L. Comparison of simple potential functions for simulating liquid water. *J. Chem. Phys.* **1983**, *79*, 926−935.

(56) Ryckaert, J.-P.; Ciccotti, G.; Berendsen, H. J. C. Numerical integration of the Cartesian equations of motion of a system with constraints: molecular dynamics of *n*-alkanes. *J. Comput. Phys.* **1977**, *23*, 327−341.

(57) Zoete, V.; Michielin, O.; Karplus, M. Relation between sequence and structure of HIV-1 protease inhibitor complexes: a model system for the analysis of protein flexibility. *J. Mol. Biol.* **2002**, *315*, 21−52.

(58) Roberts, N. A.; Martin, J. A.; Kinchington, D.; Broadhurst, A. V.; Craig, J. C.; Duncan, I. B.; Galpin, S. A.; Handa, B. K.; Kay, J.; Krohn, A.; Lambert, R. W.; Merrett, J. H.; Millis, J. S.; Parkes, K. E. B.; Redshaw, S.; Ritchie, A. J.; Taylor, D. L.; Thomas, G. J.; Machin, P. J. Rational design of peptide-based HIV proteinase inhibitors. *Science* **1990**, *248*, 358−361.

(59) Krohn, A.; Redshaw, S.; Ritchie, J. C.; Graves, B. J.; Hatada, M. H. Novel binding mode of highly potent HIV-proteinase inhibitors incorporating the (*R*)-hydroxyethylamine isostere. *J. Med. Chem.* **1991**, *34*, 3340−3342.

(60) Okimoto, N.; Tsukui, T.; Hata, M.; Hoshino, T.; Tsuda, M. Hydrolysis mechanism of the phenylalanine−proline peptide bond specific to HIV-1 protease: Investigation by the ab initio molecular orbital method. *J. Am. Chem. Soc.* **1999**, *121*, 7349−7354.

(61) Srinivasan, J.; Cheatham, T. E., III; Kollman, P.; Case, D. A. Continuum solvent studies of the stability of DNA, RNA, and phosphoramidate−DNA helices. *J. Am. Chem. Soc.* **1998**, *120*, 9401−9409.

(62) Kollman, P. A.; Massova, I.; Reyes, C.; Kuhn, B.; Huo. S.; Chong, L.; Lee, M.; Lee, T.; Duan, Y.; Wang, W.; Donini, O.; Cieplak, P.; Srinivasan, J.; Case, D. A.; Cheatham, T. E., III. Calculating structures and free energies of complex molecules: Combining molecular mechanics and continuum models. *Acc. Chem. Res.* **2000**, *33*, 889−897.
(63) Wang, W.; Kollman, P. A. Free energy calculations on dimer stability of the HIV protease using molecular dynamics and a continuum solvent model. *J. Mol. Biol.* **2000**, *303*, 567−582.
(64) Kollman, P. Free energy calculations: Applications to chemical and biochemical phenomena. *Chem. Rev.* **1993**, *93*, 2395−2417.
(65) Massova, I.; Kollman, P. A. Combined molecular mechanical and continuum solvent approach (MM-PBSA/GBSA) to predict ligand binding. *Perspect. Drug Discovery Des.* **2000**, *18*, 113−135.
(66) Onufriev, A.; Bashford, D.; Case, D. A. Exploring protein native states and large-scale conformational changes with a modified generalized born model. *Proteins: Struct., Funct., Bioinf.* **2004**, *55*, 383−394.

JM061158I

doi:10.1016/j.jmb.2007.04.081 J. Mol. Biol. (2007) 370, 598–607

JMB Available online at www.sciencedirect.com ScienceDirect ELSEVIER

Computational Characterization of Structural Role of the Non-active Site Mutation M36I of Human Immunodeficiency Virus Type 1 Protease

Hirotaka Ode[1]*, Shou Matsuyama[1], Masayuki Hata[1], Saburo Neya[1] Junko Kakizawa[2], Wataru Sugiura[2] and Tyuji Hoshino[1,3]

[1]*Graduate School of Pharmaceutical Sciences Chiba University 1-33 Yayoi-cho, Inage-ku Chiba 263-8522, Japan*

[2]*AIDS Research Center National Institute of Infectious Diseases, 4-7-1 Gakuen Musashimurayama Tokyo 208-1011, Japan*

[3]*PRESTO, JST, 4-1-8 Honcho Kawaguchi, Saitama 332-0012 Japan*

**Corresponding author*

A prominent characteristic of human immunodeficiency virus type 1 (HIV-1) is its high genetic variability, which generates diversity of the virus and often causes a serious problem of the emergence of drug-resistant mutants. Subtype B HIV-1 is dominant in advanced countries, and the mortality rate due to subtype B HIV-1 has been decreased during the past decade. In contrast, the number of patients with non-subtype B viruses is still increasing in developing countries. One of the reasons for the prevalence of non-subtype B viruses is lack of information about the biological and therapeutic differences between subtype B and non-subtype B viruses. M36I is the most frequently observed polymorphism in non-subtype B HIV-1 proteases. However, since the 36th residue is located at a non-active site of the protease and has no direct interaction with any ligands, the structural role of M36I remains unclear. Here, we performed molecular dynamics (MD) simulations of M36I protease in complex with nelfinavir and revealed the influence of the M36I mutation. The results show that M36I regulates the size of the binding cavity of the protease. The reason for the rare emergence of D30N variants in non-subtype B HIV-1 proteases was also clarified from our computational analysis.

Keywords: HIV-1; protease; resistance; M36I; non-active site mutation

Introduction

Human immunodeficiency virus type 1 (HIV-1) is one of the most hazardous viruses for humans. HIV-1 has a high genetic variability and has been classified into three groups: M, N, and O groups. Viruses in group M are further subdivided into subtypes, and circulating recombinant forms (CRFs). The subtype B virus is commonly found in HIV-1-infected patients in North America, Europe, and Japan. Some anti-HIV-1 drugs that target viral proteins (reverse transcriptase, aspartic protease, and fusion proteins) have been clinically used and have lowered the death rate due to acquired immune deficiency syndrome (AIDS) in advanced countries during the past decade. In contrast, developing countries are suffering from a growing epidemic of non-subtype B viruses. The number of patients infected with HIV-1 is still increasing in developing countries.[1]

HIV-1 proliferates under the assistance of its own aspartic protease, so-called HIV-1 protease (HIV-1 PR), in its life cycle.[2] HIV-1 PR is an enzyme composed of two identical polypeptides, each of which consists of 99 amino acid residues (Figure 1(a)), and has a function to process the viral Gag and Gag-Pol polyprotein precursors. Because this processing is essential for viral maturation, inhibition of the PR function leads to incomplete viral replication and prevents the transfer to other human cells.[3] Therefore, HIV-1 PR is an attractive target for anti-HIV-1 drugs. Nine PR inhibitors (PIs) have been approved by the Food and Drug Administration (FDA).[4–12] Nevertheless, the currently available PIs were developed and tested only against subtype B PRs. Some studies have shown that non-subtype B viruses show different responses than the responses of subtype B virus

Abbreviations used: HIV-1, human immunodeficiency virus type 1; PR, protease; PI, protease inhibitor; NFV, nelfinavir; FDA, Food and Drug Administration; WT, wild-type; MD, molecular dynamics.

E-mail address of the corresponding author: odehir@graduate.chiba-u.jp

0022-2836/$ - see front matter

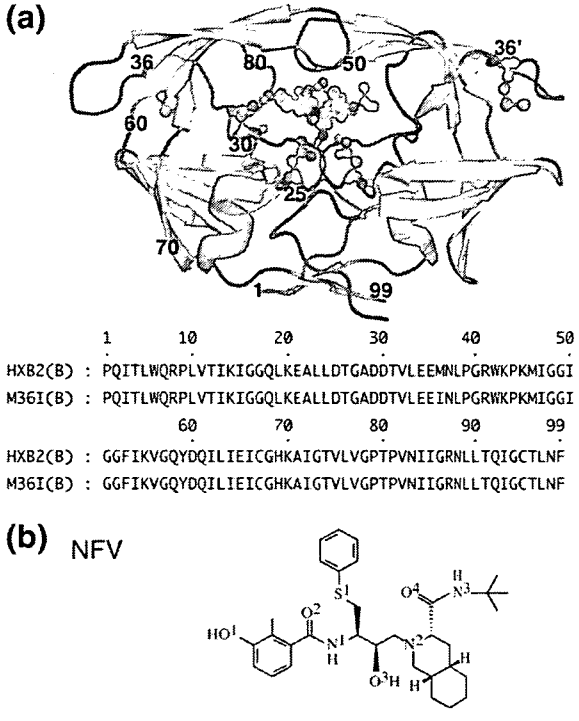

Figure 1. (a) Structure of HIV-1 PR in complex with NFV. Locations of two catalytic aspartate residues, the 30th and the 36th residues, and NFV are shown in ball and stick representations. The amino acid sequence of subtype B wild-type (WT) HIV-1 PR (HXB2) and that of M36I mutant are shown under the structure. (b) Chemical structure of NFV.

to those PIs.[13–18] Ariyoshi *et al.* reported that the patterns of emergence of resistant mutations against nelfinavir (NFV, Figure 1(b)) differed between subtype B and CRF01_AE HIV-1.[17] D30N predominantly appears in patients who are infected with subtype B HIV-1, and treatment with NFV has failed. D30N specifically confers resistance against NFV.[19,20] In contrast, N88S predominantly appears in patients with CRF01_AE HIV-1. D30N is not found in patients with CRF01_AE HIV-1. D30N has also rarely been found in patients with other non-subtype B HIV-1.[21–24] However, there have been few studies on the susceptibility of non-subtype B viruses to the presently available PIs, and a standard protocol of chemotherapy for non-subtype B viruses has not yet been established.[25]

Non-subtype B HIV-1 PRs have natural polymorphisms. Among those polymorphisms, M36I is the most frequently observed in patients with non-subtype B HIV-1.[24,26,27] M36I is known to be related to resistance against some FDA-approved PIs: NFV, indinavir, ritonavir, and atazanavir.[20] Therefore, M36I is a key mutation to understand the difference between subtype B and non-subtype B HIV-1 PRs. Nevertheless, the structural role of the non-active site mutation M36I remains unclear. This is because the 36th residue of PR is not located at the active site of PR and has no direct interaction with any substrates or any PIs.

Here, we investigated the structural role of M36I of PR in the binding of PR with NFV through computational simulations. We also examined the structural role of M36V in order to compare the effect of the side-chain at the 36th residue. Some previous computational simulations have revealed structural roles of non-active site mutations of HIV-1 PR.[28–34] Our simulations indicated that the mutations at the 36th residues influence the volume of the binding cavity of the active site of PR. The influence on the volume alters the interaction between D30 of PR and NFV. We also investigated the relationship between D30N and the mutation at the 36th residue of PR. Our results revealed that a combination of D30N and the mutation at the 36th residue induces the formation of hydrogen bonds between N30 of PR and NFV, which are not observed in PR with a single D30N mutation in complex with NFV. Our simulations suggest that M36I, despite the fact that it is a mutation at a non-active site, regulates the binding of ligands with PR. These findings will be helpful for developing more effective PIs against non-subtype B HIV-1.

Results

Hydrogen bond networks

We performed MD simulations of six subtype B HIV-1 PRs in complex with NFV: wild-type (WT) PR, M36I PR, M36V PR, D30N PR, D30N/M36I PR, and D30N/M36V PR (labeled as B(WT), B(M36I), B(M36V), B(D30N), B(D30N/M36I), and B(D30N/M36V), respectively). First, in order to clarify the structural role of the mutation at the 36th residue, we examined direct or one-water-molecule-mediated hydrogen bonds between each PR and NFV (Table 1, Supplementary Data Table S1). According to the X-ray structure of HIV-1 PR bound to NFV,[35] NFV has direct and one-water-molecule-mediated hydrogen bonds with D25/D25′, I50/I50′, D29′, and D30 (Supplementary Data Figure S1). In all of the six models, the side-chains of D25 and D25′ directly interacted with the central hydroxyl group of NFV (O3 in Figure 1(b)). All of models also have one-water-molecule-mediated hydrogen bonds of NFV with I50/I50′ and with D29′. Different hydrogen bonds are observed between the 30th residue and the phenol group of NFV. In B(WT) and B(M36V), either the main chain or the side-chain of D30 interacts with NFV through hydrogen bonds (Figure 2). In B(M36I), only the side-chain of D30 forms a hydrogen bond with NFV. In contrast, B(D30N) has no hydrogen bond with NFV. B(D30N/M36I) and B(D30N/M36V) show a different feature from that of B(D30N). They have direct hydrogen bonds between the main chain of N30 and NFV.

Change in conformation of PR

Next, we investigated the difference in the average structure of each PR from that of B(WT). The average structure of each PR was generated from 1000 snapshot structures during the last 1.0 ns of molecular dynamics (MD) simulations. In order to

Table 1. Hydrogen bond networks of NFV with D30 or N30 in PR

Donor		Acceptor		%[a]	Donor		Acceptor		%
		WT					D30N		
N	D30	O1[b]	NFV	30.7					
O1	NFV	OD1/OD2	D30	31.6					
O1	NFV	O	D30	42.9					
		M36I					D30N/M36I		
O1	NFV	OD2	D30	95.3	O1	NFV	O	N30	57.1
		M36V					D30N/M36V		
N	D30	O1	NFV	18.0	N	N30	O1	NFV	24.9
O1	NFV	OD1/OD2	D30	46.1					
O1	NFV	O	D30	35.9	O1	NFV	O	N30	34.7

[a] Occupancy of hydrogen bonds during the 2.0–3.0 ns MD simulation.
[b] The atom names of NFV are shown in Figure 1.

make a comparison between each PR and B(WT), we superimposed the average structure of each PR onto that of B(WT) using the coordinates of N, C^{α}, and C atoms. Since non-active site residues are more flexible than active site residues and the structure of non-active site residues is largely influenced by random atom motions in MD simulation (Supplementary Data Figure S2), we focused on conformational change of the active site residues. Figure 3 shows that the displacements of most of the active site residues are small. Detailed values are shown in Supplementary Data Figure S3. Exceptionally, a large conformational change (RMSD=1.5 Å) is observed at D29 in B(D30N/M36I). In the other PRs, D29 is shifted about 0.7 Å. D30 is noticeably displaced by 0.8 Å in only B(D30N), while displacement of the 30th residues is less than 0.5 Å in the

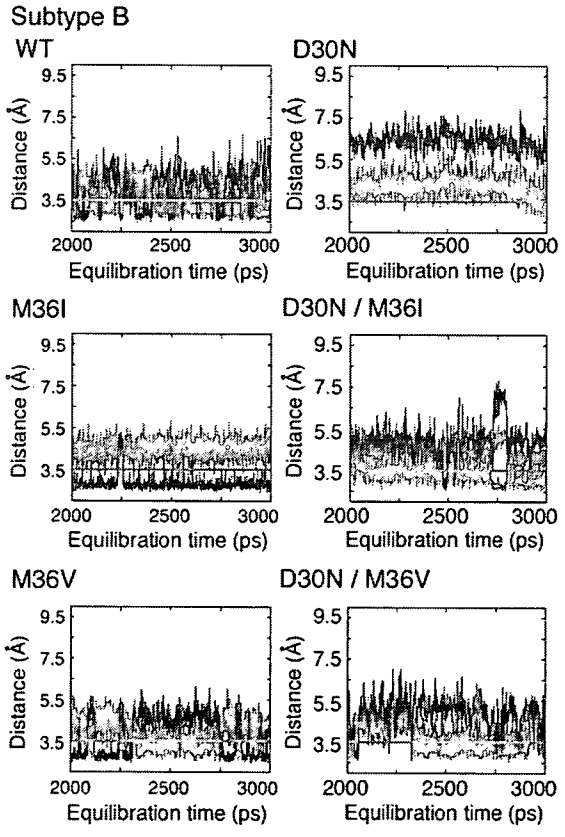

Figure 2. Distance between the 30th residue of PR and NFV. Red and green continuous lines correspond to the distance between N of the 30th residue and O1 atom of NFV and that between O of the 30th residue and O1 atom of NFV, respectively. Blue continuous lines of B(WT), B(M36I), and B(M36V) show the distance between OD1/OD2 of D30 and O1 atom of NFV, while those of B(D30N), B(D30N/M36I), and B(D30N/M36V) are the distance between OD1/ND2 of N30 and O1 atom of NFV.

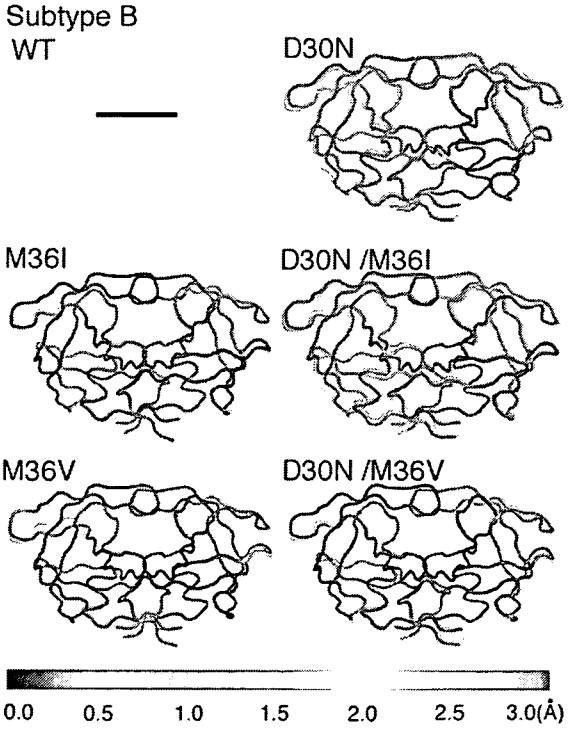

Figure 3. 3D plot of RMSD of the average structure of each model from that of B(WT). PR is shown in colored tube representations. Color indicates the magnitude of RMSD shown in the bottom bar. Each model was fitted to B(WT) using the coordinates of main chain atoms N, C^{α}, and C of PR. The superimposed gray tubes represent the average structure of B(WT).

Table 2. Volume and surface area of the binding cavity in each model

	WT	M36I	M36V	D30N	D30N/M36I	D30N/M36V
Volume (Å^3)	375(±43)[a]	345(±36)	365(±43)	403(±53)	419(±53)	375(±47)
Surface area (Å^2)	490(±43)	471(±35)	469(±47)	508(±40)	506(±54)	484(±48)

[a] The standard deviations were written in the parentheses.

other PRs. At a flap region and around 80s loops, slight conformational changes are also observed. The flap and 80s loop consist of the 47th to 50th residues and of the 79th to 81st residues, respectively. Although HIV-1 PR is a homodimer, the asymmetric displacements are observed. The displacement in NFV was also examined (Supplementary Data Figure S4). Conformational changes in the benzamide group and the S-phenyl group (C6H6-S-) are observed. B(D30N) and B(D30N/M36I) show larger displacement than that of the other models. In contrast, the *tert*-butylcarboxamide moiety and the dodecahydroisoquinoline ring hardly change their locations in each model. The displacements of NFV are also asymmetric and correlate with the displacements of PR. The residues near the benzamide group of NFV, such as the 29th and 30th residues, show large displacement. On the other hand, the residues near the *tert*-butylcarboxamide moiety or the dodecahydroisoquinoline ring of NFV show small displacements. The asymmetric displacements observed in HIV-1 PR will be due to the structural collision with NFV.

Furthermore, we examined the effect of the mutation at the 36th residue on volume of the active site (Table 2). M36I reduces the volume of the active site, whereas both D30N and D30N/M36I increase it. M36V and D30N/M36V have almost no effect on the volume.

Binding energy calculations

Binding energy between each PR and NFV is presented in Table 3. A single M36I or M36V mutation has almost no effect on the binding affinity with NFV, although the binding energy calculations have large standard deviations. In contrast, D30N and D30N/M36I mutations reduce the binding energies with NFV. Oppositely, D30N/M36V increases the affinity. Clemente *et al.* reported the IC50 values of B(WT), B(D30N), B(M36I), and B(D30N/M36I),[36] in which M36I was suggested to improve the binding affinity with NFV, and showed that D30N/M36I conferred resistance against NFV. Our results are compatible with those experimental results.

We additionally analyzed the contribution of each residue to the binding of NFV (Supplementary Data Figure S5). In B(M36I), B(M36V), and B(D30N/M36V), the respective residues except D25/D25' have contributions similar to those in B(WT). The contribution of D25/D25' depends on their protonation states. In contrast, B(D30N) reduces the binding energy between the 30th residue and NFV. B(D30N/M36I) lowers the interaction between D29 and NFV.

Discussion

Here, we performed MD simulations of HIV-1 PRs in complex with NFV for the purpose of clarifying (1) the structural role of the non-active site mutation M36I and (2) the relationship between D30N and M36I mutations. M36V was also examined in order to analyze the effect of the side-chain of the 36th residue.

Non-subtype B HIV-1 is still pandemic in the world.[1] Nevertheless, a standard protocol of chemotherapy for non-subtype B viruses has not yet been established,[25] and little is known about the difference between susceptibilities of non-subtype B viruses and subtype B virus to clinically available drugs.[13–18] M36I is the most frequently observed polymorphism among non-subtype B HIV-1 PRs.[24,26,27] Therefore, M36I is a key mutation to clarify the reason why the efficacy of PIs varies among subtypes. Some studies have indicated that M36I is related to the resistance against NFV and other FDA-approved PIs by complementing the effects of other resistant mutations.[17,20,34,36] For example, M36I has been shown to contribute to an increase in the emergence rate of the NFV-resistant mutation N88S.[17,34] It has also been reported that a

Table 3. Binding free energy of each model

	ΔG_{int}^{ele} (kcal/mol)	ΔG_{int}^{vdw} (kcal/mol)	ΔG_{sol} (kcal/mol)	ΔG_b[a] (kcal/mol)	$\Delta\Delta G_b$ (kcal/mol)	IC50[b] (nM)
WT	−12.5±1.4	−71.8±3.8	15.1±1.4	−69.2±3.7	-	1.2±0.2
M36I	−11.8±1.2	−73.3±3.7	15.4±1.1	−69.7±3.5	−0.5	0.9±0.1
M36V	−13.2±1.5	−72.1±3.8	16.5±1.3	−68.8±3.6	0.4	ND[c]
D30N	−6.9±1.2	−70.5±4.1	10.9±0.9	−66.5±3.9	2.7	6.8±0.9
D30N/M36I	−8.1±1.2	−66.8±3.6	9.8±1.1	−65.0±3.5	4.2	6.0±1.0
D30N/M36V	−10.8±1.2	−72.8±3.9	13.3±1.0	−70.3±4.0	−1.1	ND

[a] $T\Delta S$ is not included.
[b] Reference from the report by Clemente *et al.*[35]
[c] ND denotes no data.

single M36I mutation does not confer resistance against FDA-approved PIs.[36] The structural role of M36I is, however, not clear because the 36th residue of PR is located at a non-active site of HIV-1 PR. According to the results of the present simulations, a single M36I mutation reduces the volume of the binding cavity of subtype B HIV-1 PR. Energetically, M36I PR slightly increases the binding affinity with NFV, compared with WT PR. This result is compatible with an experimental finding.[36] A single M36V mutation also reduces the volume of the cavity, although the effect of M36V on the cavity volume is not as great as that of M36I. When we carried out an additional 2.0 ns MD simulation of each model, the reduction of the volume of the active site of M36I PR and that of M36V PR were also observed (Supplementary Data Table S2). Therefore, the side-chain of the 36th residue will indeed influence the shape of the active site of PR, despite its location.

In order to reveal the mechanism by which the non-active site mutation M36I regulates the volume of the active site of PR, we additionally calculated the interaction energy between each residue of PR and the 36th residue. The energy calculations suggest that the 36th residue mainly interacts with I15/I15′, Q18/Q18′, K20/K20′, L33/L33′, and V77/V77′ (Supplementary Datal Figure S6). Among these residues, L33/L33′ and V77/V77′ are located near active site residues (Figure 4). V77/V77′ is close to the 80s loop, which consists of the residues from P79/P79′ to P81/P81′. L33/L33′ is in the vicinity of T31/T31′. Interestingly, mutations at L33 and V77 (L33F and V77I) are also related to the resistance against some PIs.[20] These mutations would play a role similar to that of M36I. We speculate that the

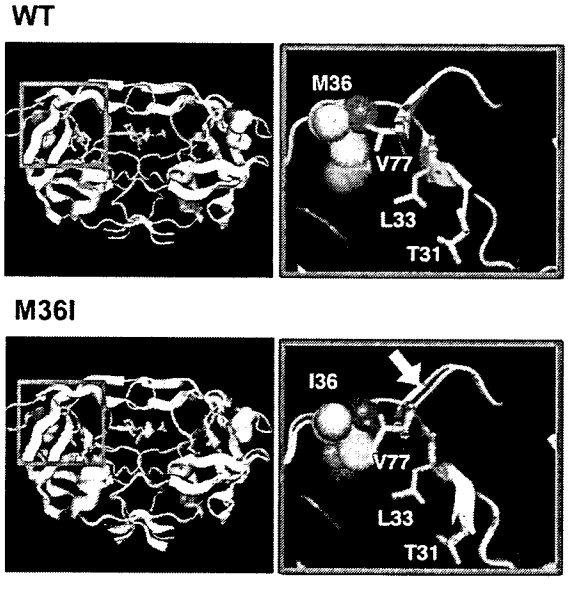

Figure 4. Interactions of the 36th residues with L33 and with V77. The average structure of B(WT) was superimposed onto that of B(M36I) using the coordinates of N, C^{α}, and C atoms. The superimposed structure of B(WT) is shown in gray sticks and cartoons representation. The orange arrow indicates the locations of the 80s loop, where a prominent change of conformation occurred by M36I.

slight inward shifts of L33/L33′ and V77/V77′ due to the mutation M36I trigger the reduction in volume of the cavity of PR. In order to confirm this speculation, we further examined the shift of each residue and extracted the shift only toward the center of the active site (Figure 5, Supplementary Data Figures S7–S9). The results show that M36I causes a shrinkage of the active site around P79 and around T31′. The 31st residue T31/T31′ creates stable hydrogen bond networks with D29, T74, and N88 or with D29′, T74′, and N88′ (Supplementary Data Table S3).[28,34] also indirectly influences the conformations around D29/D29′. A28′, D29′, D30′, and T31′ in one monomer are all displaced inward. In contrast, A28 and D29 show outward positional shifts, while the residues around L33 in the other monomer move inward. It is notable that these residues rotate on D30. M36I hardly shrinks or expands the cavity at D30. However, D30 shifts toward the α-helix region (R87–I93) in B(M36I) (Supplementary Data Figure S10). Although this displacement is very slight (0.4 Å), the shift enlarges the distance from the main chain of D30 to the *m*-phenol group of NFV, and it also shortens the distance from the side-chain of D30 to NFV (Figure 2). Therefore, M36I changes the interaction between D30 and NFV. D30 is an important residue for binding with NFV.[28,34,35] B(M36I) has a hydrogen bond of the *m*-phenol group of NFV only with the side-chain of D30, unlike B(WT). B(WT) forms hydrogen bonds of the *m*-phenol group of NFV with either the main chain or the side-chain of D30. These results show that the non-active site mutation M36I influences the shape of the active site of PR by the following mechanism. M36I mutation shifts L33/L33′ and V77/V77′ inward. Subsequently, these shifts cause changes in conformation at the active site, especially around T31/T31′ and P79/P79′.

It is also informative to investigate the relationship between D30N and M36I. As stated in Introduction, most of the non-subtype B HIV-1 PRs carry M36I as a polymorphism.[24,26,27] In contrast, D30N rarely appears in non-subtype B HIV-1 PRs.[21–24] This rare emergence of D30N in non-subtype B PRs has been assumed to be due to the low viral replication ability of D30N mutants in non-subtype B viruses,[22,37] because L89M, which is a polymorphism of some non-subtype B PRs, and D30N decrease the replication ability.[22,37] On the other hand, our simulations provide a novel insight into the relationship between D30N and M36I. It should be noted that B (D30N/M36I) forms a hydrogen bond between the main chain of N30 and NFV (Figure 2), which is not seen in B(D30N). M36I enforces the interaction between N30 and NFV in D30N mutant PR. A clear difference is observed at D29 among B(WT), B (M36I), B(D30N), and B(D30N/M36I) (Figure 5). D29 in B(D30N/M36I) shows a large outward positional shift from that of B(WT). The shift of B (D30N/M36I) is two-times larger than that of B (M36I) and B(D30N). Binding energy calculations show that D30N/M36I lowers the binding affinity of NFV with subtype B PR (Table 3) and greatly

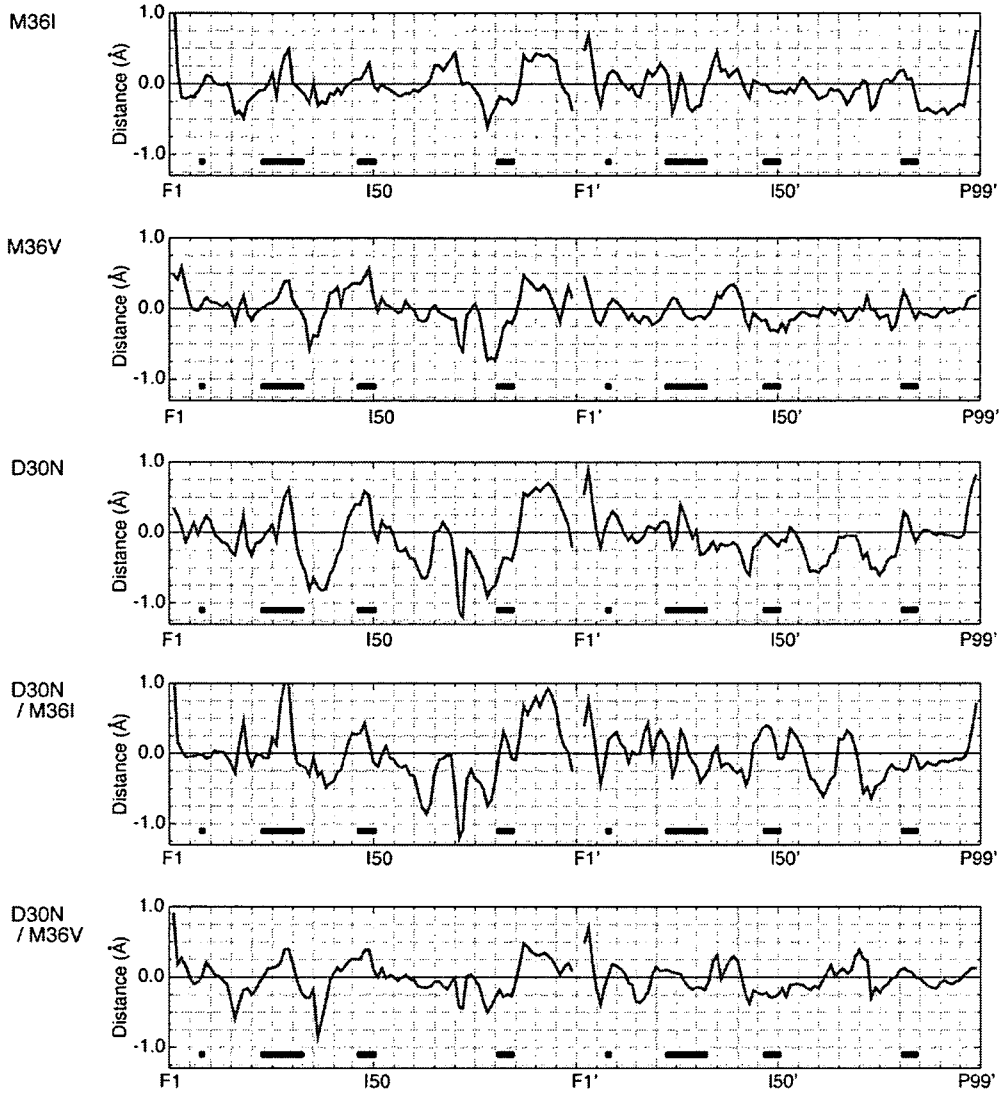

Figure 5. Positional shift of each residue measured from the center of the binding cavity in the average coordinate of WT PR. Negative values indicate contraction of distances measured from the center of the cavity, and positive values indicate elongation of the distances. Bottom black lines represent the locations of the active site residues.

reduces the interaction between D29 and NFV. D30N/M36I mutant of subtype B PR was reported to confer resistance against NFV.[36] This energetical result is compatible with experimental findings.[36] These results suggest that the resistance mechanism due to D30N/M36I is different from that of D30N. D30N causes resistance against NFV because of the loss of hydrogen bonds between N30 and NFV.[28,34] On the other hand, D30N/M36I confers resistance against NFV due to the large change in conformation at D29. NFV still interacts with N30 in B(D30N/M36I). It is known that D30N is not observed in CRF01_AE PR.[17] As we previously reported,[34] this observation is explained by the finding that the affinity of CRF01_AE D30N PR with NFV is similar to that of CRF01_AE reference PR. CRF01_AE D30N PR has stronger interaction with NFV than does subtype B D30N PR. CRF01_AE D30N PR has one-water-molecule-mediated hydrogen bonds between NFV and N30, whereas subtype B D30N PR forms no hydrogen bond between them. M36I enforces the interaction between N30 and NFV, and polymorphisms other than M36I will release the distortion at D29. NFV will be able to maintain its efficacy against D30N mutant PR in non-subtype B viruses. Therefore, D30N mutation is rarely observed in non-subtype B HIV-1 PRs.

Here, we performed MD simulations of six HIV-1 PRs in complex with NFV and clarified the structural role of the non-active site mutation M36I. M36I influences the shape of the active site of PR in spite of its location. The changes in conformation at the active site are caused by the alteration of interaction of the 36th residue with L33 and V77. We also examined the relationship between D30N and M36I. A combination of D30N and M36I enforces the interaction between N30 and NFV, causing distortion on the conformation around D29. D30N/M36I shows a different mechanism of resistance against NFV from that of D30N. M36I is the most frequently observed mutation in non-subtype B PRs. Therefore, M36I is a key mutation to understand the differences

between subtype B and non-subtype B PRs. The findings of this study provide valuable information for developing the drugs that are more effective for non-subtype B PRs. Furthermore, accumulation of information on structural roles of key residues of PR will enable us to predict the effectiveness of PIs against non-subtype B viruses as well as against subtype B ones.

Materials and Methods

Molecular dynamics simulation

We performed minimizations and MD simulations in a manner similar to that described elsewhere.[34] Minimizations and MD simulations were carried out using the Sander module of the AMBER8 package.[38] The AMBER ff03 force field[39] was used as the parameters for proteins, ions, and water molecules. Our originally developed torsion parameters for the benzamide moiety in NFV, CA-CA-C –N and CA-CA-C –O, were applied.[34] The general AMBER force field[40] was used as other parameters for NFV. RESP charges for NFV were determined on the basis of data obtained from quantum chemical calculations.[34]

We performed simulations of six proteases in complex with NFV: wild-type (WT) PR, M36I PR, M36V PR, D30N PR, D30N/M36I PR, and D30N/M36V PR of subtype B HIV-1 (labeled as B(WT), B(M36I), B(M36V), B(D30N), B(D30N/M36I), and B(D30N/M36V), respectively). B(M36V) and B(D30N/M36V) were examined in order to analyze the effect of the side-chain of the 36th residue clearly. We used HXB2 as the WT sequence of subtype B HIV-1. Each initial structure for the PR in complex with NFV was modeled from the atom coordinates of an X-ray crystal structure (PDB code: 1OHR[35]) and the respective mutations were introduced using the LEaP module. First, we obtained the PDB file of the PR bound to NFV from Protein Data Bank†. Second, we edited the PDB file to change the residue names of the mutated residues and to delete the information on the coordinates of the side-chain atoms of the mutated residues. Third, the coordinates of the side-chain atoms of the mutated residues were automatically generated by LEaP module. Fourth, each model was placed in a rectangular box filled with about 8000 TIP3P water molecules,[41] with all of the crystal water molecules remaining. The cutoff distance for the long-range electrostatic and the van der Waals energy terms was set to 12.0 Å. The expansion and shrinkage of all covalent bonds connecting to a hydrogen atom were constrained using the SHAKE algorithm.[42] Periodic boundary conditions were applied to avoid the edge effect in all calculations. Energy minimization was achieved in three steps. First, movement was allowed only for water molecules and ions. Next, the ligand and the mutated residues were allowed to move in addition to the water molecules and ions. In this step, steric collisions of the automatically generated residues were minimized and favorable configurations of the side-chains of the mutated residues were obtained. Finally, all atoms were permitted to move freely. In each step, energy minimization was executed by the steepest descent method for the first 10,000 cycles and the conjugated gradient method for the subsequent 10,000 cycles. After a 0.1 ns heating calculation until 310 K using the NVT ensemble, a 3.0 ns equilibrating calculation was executed at 1 atm and at 310 K using the NPT ensemble, with an integration time step of 2.0 fs. In the present calculations, the MD simulations showed no large fluctuations after about 2.0 ns equilibrating calculation (Supplementary Data Figures S11 and S12). Hence, atom coordinates were collected at intervals of 1.0 ps for the last 1.0 ns to analyze the structure in detail. Furthermore, we performed an additional 2.0 ns simulation for each model and confirmed equilibrium of each simulation (Supplementary Data Figure S13).

Protonation states of the catalytic aspartic acids D25 and D25′ vary depending on the binding ligands or PRs.[43] Hence, appropriate protonation states of the catalytic aspartic acids should be determined for each model. Since NFV mimics a transition state of catalytic reaction by HIV-1 PR, we considered two kinds of protonation states.[44–46] One complex represented a combination of protonated D25/unprotonated D25′ states, and the other represented the opposite combination. In order to determine the protonation states when NFV is bound to each PR, the free energies of two kinds of complexes were compared using calculation data obtained during the 2.0–3.0 ns MD simulations (Supplementary Data Table S4). The free energies were calculated on the basis of the MM/PBSA method.[47,48] We used the same parameter set for electrostatic and van der Waals energy terms as that used in the MD simulations, and no cutoff was applied for the calculation. Since the dielectric constants for the interior of proteins is considered to be in the range of 2 to 4, the interior dielectric constant was set to 2.0.[49] The outer dielectric constant was set to 80.0. The pbsa program was used to solve the Poisson-Boltzmman (PB) equation. B(D30N), B(M36I), and B(D30N/M36I) have been found to favor the combination of protonated D25 and unprotonated D25′. The other three PRs, B(WT), B(M36V) and B(D30N/M36V), prefer the combination of unprotonated D25 and protonated D25′.

Hydrogen bond criteria

The formation of a hydrogen bond was defined in terms of distance and orientation. The combination of donor D, hydrogen H, and acceptor A atoms with a D - H ... A configuration was regarded as a hydrogen bond when the distance between donor D and acceptor A was shorter than 3.5 Å and the angle H-D-A was smaller than 60.0 degrees.

Calculations of volume and surface area of the binding cavity

We employed the Pocket program[50] to estimate the volume and the surface area of the active site of PR. The program is based on the Alpha Shape theory,[50] which provides an analytical method for detecting pockets in proteins and measuring their volume and surface area. The ligand-binding cavity of HIV-1 PR is not completely separated from solvent. However, it should be noted that, in the Pocket program, a pocket is defined as a cavity that is inaccessible to the solvent outside of a protein. If a water molecule is trapped within the pocket, the water molecule cannot escape to the outside of the protein. Hence, we can define the ligand-binding cavity as a pocket. Supplementary Data Figure S14 shows the binding pocket of HIV-1 PR visualized by MAGE program.[51]

† http://www.pdb.org/

Binding free energy calculation

The binding free energy[52] was calculated by the following equation:

$$\Delta G_b = \Delta G_{int}^{ele} + \Delta G_{int}^{vdw} + \Delta G_{sol} - T\Delta S,$$

where ΔG_b is the binding free energy in solution, ΔG_{int}^{ele} and ΔG_{int}^{vdw} are the electrostatic and van der Waals interaction energies between a ligand and a protein, ΔG_{sol} is the solvation energy, and $-T\Delta S$ is the contribution of conformational entropy to the binding. Here, assuming that the contribution of conformational entropy to the change in ΔG_b is negligible among mutants,[53] we disregarded the entropy term in the energy estimation. ΔG_{int}^{ele} and ΔG_{int}^{vdw} were computed using the same parameter set as that used in the MD simulation, and no cutoff was applied for the calculation. Solvation energy ΔG_{sol} was calculated using the pbsa program. The interior dielectric constant was set to 2.0[49] and the outer dielectric constant was set to 80.0. Furthermore, the contribution of each residue to the binding free energy was calculated. The total binding free energy was decomposed into the contribution from each individual residue by the MM/GBSA method. The modified GB model developed by Onufriev *et al.*[54] was used to calculate the solvation energy term. The MM/GBSA results were highly correlated with the MM/PBSA results, as we described previously.[34]

Acknowledgements

This work was supported by a Health and Labor Science Research Grant for Research on HIV/AIDS from the Ministry of Health and Labor of Japan and by JSPS Research Fellowships for Young Scientists and a grant-in-aid for JSPS Fellows. A part of this work was also supported by a grant-in-aid from Japan Society for the Promotion of Science, No. 19590467, and by a grant from the Japan Science and Technology Agency.

Supplementary Data

Supplementary data associated with this article can be found, in the online version, at doi:10.1016/j.jmb.2007.04.081

References

1. Joint United Nations Programme on HIV/AIDS (UNAIDS). (2006). 2006 Report on the Global AIDS Epidemic. *UNAIDS*, Geneva, Switzerland.
2. Krausslich, H. G. & Wimmer, E. (1988). Viral proteinases. *Annu. Rev. Biochem.* **57**, 701–754.
3. Kohl, N. E., Emini, E. A., Schleif, W. A., Davis, L. J., Heimbach, J. C., Dixon, R. A. *et al.* (1988). Active human immunodeficiency virus protease is required for viral infectivity. *Proc. Natl Acad. Sci. USA*, **85**, 4686–4690.
4. Craig, J. C., Duncan, I. B., Hockley, D., Grief, C., Roberts, N. A. & Mills, J. S. (1991). Antiviral properties of Ro 31-8959, an inhibitor of human immunodeficiency virus (HIV) proteinase. *Antiviral Res.* **16**, 295–305.
5. Vacca, J. P., Dorsey, B. D., Schleif, W. A., Leven, R. B., McDaniel, S. L., Darke, P. L. *et al.* (1994). L-735,524: an orally bioavailable human immunodeficiency virus type 1 protease inhibitor. *Proc. Natl Acad. Sci. USA*, **91**, 4096–4100.
6. Kempf, D. J., Marsh, K. C., Denissen, J. F., McDonald, E., Vasavanonda, S., Flentga, C. A. *et al.* (1995). ABT-538 is a potent inhibitor of human immunodeficiency virus protease and has high oral bioavailability in humans. *Proc. Natl Acad. Sci. USA*, **92**, 2484–2488.
7. Livington, D. J., Pazhanisamy, S., Porter, D. J., Partaledis, J. A., Tung, R. D. & Painter, G. R. (1995). Weak binding of VX-478 to human plasma proteins and implications for anti-human immunodeficiency virus therapy. *J. Infect. Dis.* **172**, 1238–1245.
8. Patick, A. K., Mo, H., Markowitz, M., Appelt, K., Wu, B., Musick, L. *et al.* (1996). Antiviral and resistance studies of AG1343, an orally bioavailable inhibitor of human immunodeficiency virus protease. *Antimicrob. Agents Chemother.* **40**, 292–297 (Erratum, **40**, 1575).
9. Carrillo, A., Stewart, K. D., Sham, H. L., Norbeck, D. W., Kohlbrenner, W. E., Leonard, J. M. *et al.* (1998). In vitro selection and characterization of human immunodeficiency virus type 1 variants with increased resistance to ABT-378, a novel protease inhibitor. *J. Virol.* **72**, 7532–7541.
10. Robinson, B. S., Riccardi, K. A., Gong, Y. F., Guo, Q., Stock, D. A., Blair, W. S. *et al.* (2000). BMS-232632, a highly potent human immunodeficiency virus protease inhibitor that can be used in combination with other available antiretroviral agents. *Antimicrob. Agents Chemother.* **44**, 2093–2099.
11. Larder, B. A., Hertogs, K., Bloor, S., van den Eynde, C., DeCian, W., Wang, Y. *et al.* (2000). Tipranavir inhibits broadly protease inhibitor-resistant HIV-1 clinical samples. *AIDS*, **14**, 1943–1948.
12. Koh, Y., Nakata, H., Maeda, K., Ogata, H., Bilcer, G., Devasamudram, T. *et al.* (2003). Novel bis-tetrahydrofuranylurethane-containing nonpeptidic protease inhibitor (PI) UIC-94017 (TMC114) with potent activity against multi-PI-resistant human immunodeficiency virus in vitro. *Antimicrob. Agents Chemother.* **47**, 3123–3129.
13. Cornelissen, M., van den Burg, R., Zorgdrager, F., Lukashov, V. & Goudsmit, J. (1997). pol gene diversity of five human immunodeficiency virus type 1 subtypes: evidence for naturally occurring mutations that contribute to drug resistance, limited recombination patterns, and common ancestry for subtypes B and D. *J. Virol.* **71**, 6348–6358.
14. Pieniazek, D., Rayfield, M., Hu, D. J., Nkengasong, J., Wiktor, S. Z., Downing, R. *et al.* (2000). Protease sequences from HIV-1 group M subtypes A-H reveal distinct amino acid mutation patterns associated with protease resistance in protease inhibitor-naive individuals worldwide. HIV variant working group. *AIDS*, **14**, 1489–1495.
15. Vergne, L., Peeters, M., Mpoudi-Ngole, E., Bourgeois, A., Liegeois, F., Toure-Kane, C. *et al.* (2000). Genetic diversity of protease and reverse transcriptase sequences in non-subtype-B human immunodeficiency virus type 1 strains: evidence of many minor drug resistance mutations in treatment-naive patients. *J. Clin. Microbiol.* **38**, 3919–3925.
16. Grossman, Z., Vardinon, N., Chemtob, D., Alkan, M. L., Bentwich, Z., Burke, M. *et al.* (2001). Genotypic variation of HIV-1 reverse transcriptase and protease:

comparative analysis of clade C and clade B. *AIDS*, **15**, 1453–1460, (Erratum, **15**, 2209).
17. Ariyoshi, K., Matsuda, M., Miura, H., Tateishi, S., Yamada, K. & Sugiura, W. (2003). Patterns of point mutations associated with antiretroviral drug treatment failure in CRF01_AE (subtype E) infection differ from subtype B infection. *J. AIDS*, **33**, 336–342.
18. Clemente, J. C., Coman, R. M., Thiaville, M. M., Janka, L. K., Jeung, J. A., Nukoolkarn, S. *et al.* (2006). Analysis of HIV-1 CRF_01 A/E protease inhibitor resistance: structural determinants for maintaining sensitivity and developing resistance to atazanavir. *Biochemistry*, **45**, 5468–5477.
19. Sugiura, W., Matsuda, Z., Yokomaku, Y., Hertogs, K., Larder, B., Oishi, T. *et al.* (2002). Interference between D30N and L90M in selection and development of protease inhibitor-resistant human immunodeficiency virus type 1. *Antimicrob. Agents Chemother.* **46**, 708–715.
20. Johnson, V. A., Brun-Vézinet, F., Clotet, B., Kuritzkes, D. R., Pillay, D., Schapiro, J. M. & Richman, D. D. (2006). Update of the drug resistance mutations in HIV-1: Fall 2006. *Top. HIV Med.* **14**, 125–130.
21. Cane, P. A., Ruiter, A., Rice, P., Wiselka, M., Fox, R. & Pillay, D. (2001). Resistance-associated mutations in the human immunodeficiency virus type 1 subtype C protease gene from treated and untreated patients in the United Kingdom. *J. Clin. Microbiol.* **39**, 2652–2654.
22. Grossman, Z., Paxinos, E. E., Averbuch, D., Maayan, S., Parkin, N. T., Engelhard, D. *et al.* (2004). Mutation D30N is not preferentially selected by human immunodeficiency virus type 1 subtype C in the development of resistance to nelfinavir. *Antimicrob. Agents Chemother.* **48**, 2159–2165.
23. Gonzalez, L. M. F., Brindeiro, R. M., Aguiar, R. S., Pereira, H. S., Abreu, C. M., Soares, M. A. & Tanuri, A. (2004). Impact of nelfinavir resistance mutations on in vitro phenotype, fitness and replication capacity of human immunodeficiency virus type 1 with subtype B and C proteases. *Antimicrob. Agents Chemother.* **48**, 3552–3555.
24. Kantor, R., Katzenstein, D. A., Efron, B., Carvalho, A. P., Whynhoven, B., Cane, P. *et al.* (2005). Impact of HIV-1 subtype and antiretroviral therapy on protease and reverse transcriptase genotype: results of a global collaboration. *Pros. Med.* **2**, e112.
25. Billingam, D. (2006). Does the world need another AIDS authority? *Lancet*, **368**, 1639–1640.
26. Kantor, R. & Katzenstein, D. (2003). Polymorphism in HIV-1 non-subtype B protease and reverse transcriptase and its potential impact on drug susceptibility and drug resistance evolution. *AIDS Rev.* **5**, 25–35.
27. Nkengasong, J. N., Adje-Toure, C. & Weidle, P. J. (2004). HIV antiretroviral drug resistance in Africa. *AIDS Rev.* **6**, 4–12.
28. Ode, H., Ota, M., Neya, S., Hata, M., Sugiura, W. & Hoshino, T. (2005). Resistant mechanism against nelfinavir of human immunodeficiency virus type-1 proteases. *J. Phys. Chem. B*, **109**, 565–574.
29. Skalova, T., Dohnalek, J., Duskova, J., Petrokova, H., Hradilek, M., Soucek, M. *et al.* (2006). HIV-1 protease mutations and inhibitor modifications monitored on a series of complexes. Structural basis for the effect of the A71V mutation on the active site. *J. Med. Chem.* **49**, 5777–5784.
30. Piana, S., Carloni, P. & Rothlisberger, U. (2002). Drug resistance in HIV-1 protease: flexibility-assisted mechanism of compensatory mutations. *Protein Sci.* **11**, 2393–2402.
31. Ode, H., Neya, S., Hata, M., Sugiura, W. & Hoshino, T. (2006). Computational simulations of HIV-1 proteases-multi-drug resistance due to nonactive site mutation L90M. *J. Am. Chem. Soc.* **128**, 7887–7895.
32. Meiselbach, H., Horn, A. H. C., Harrer, T. & Sticht, H. (2006). Insights into amprenavir resistance in E35D HIV-1 protease mutation from molecular dynamics and binding free-energy calculations. *J. Mol. Model.* **13**, 297–304.
33. Batista, P. R., Wilter, A., Durham, E. H. & Pascutti, P. G. (2006). Molecular dynamics simulations applied to the study of subtypes of HIV-1 protease common to Brazil, Africa, and Asia. *Cell Biochem. Biophys.* **44**, 395–404.
34. Ode, H., Matsuyama, S., Hata, M., Hoshino, T., Kakizawa, J. & Sugiura, W. (2007). Mechanism of drug resistance due to N88S in CRF01_AE HIV-1 protease, analyzed by molecular dynamics simulations. *J. Med. Chem.* **50**, 1768–1777.
35. Clemente, J. C., Hermrajani, R., Blum, L. E., Goodenow, M. M. & Dunn, B. M. (2003). Secondary mutations M36I and A71V in the human immunodeficiency virus type 1 protease can provide an advantage for the emergence of the primary mutation D30N. *Biochemistry*, **42**, 15029–15035.
36. Kaldor, S. W., Kalish, V. J., Davies, J. F., Shetty, B. V., Fritz, J. E., Appelt, K. *et al.* (1997). Viracept (nelfinavir mesylate, AG1343): a potent, orally bioavailable inhibitor of HIV-1 protease. *J. Med. Chem.* **40**, 3979–3985.
37. Abecasis, A. B., Deforche, K., Snoeck, J., Bacheler, L. T., McKenna, P., Carvalho, A. P. *et al.* (2005). Protease mutation M89I/V is linked to therapy failure in patients infected with the HIV-1 non-B subtypes C, F or G. *AIDS*, **19**, 1799–1806.
38. Case, D. A., Darden, T. A., Cheatham, T. E. III, Simmerling, C. L., Wang, J., Duke, R. E. *et al.* (2004). *AMBER 8*, University of California, San Francisco.
39. Duan, Y., Wu, C., Chowdhury, S., Lee, M. C., Xiong, G., Zhang, W. *et al.* (2003). A point-charge force field for molecular mechanics simulations of proteins based on condensed-phase quantum mechanical calculations. *J. Comput. Chem.* **24**, 1999–2012.
40. Wang, J., Wolf, R. M., Caldwell, J. W., Kollman, P. A. & Case, D. A. (2004). Development and testing of a general Amber force field. *J. Comput. Chem.* **25**, 1157–1174.
41. Jorgensen, W. L., Chandrasekhar, J., Madura, J. D., Impey, R. W. & Klein, M. L. (1983). Comparison of simple potential functions for simulating liquid water. *J. Chem. Phys.* **79**, 926–935.
42. Ryckaert, J.-P., Ciccotti, G. & Berendsen, H. J. C. (1977). Numerical integration of the cartesian equations of motion of a system with constraints: molecular dynamics of n-alkanes. *J. Comput. Phys.* **23**, 327–341.
43. Zoete, V., Michielin, O. & Karplus, M. (2002). Relation between sequence and structure of HIV-1 protease inhibitor complexes: a model system for the analysis of protein flexibility. *J. Mol. Biol.* **315**, 21–52.
44. Roberts, N. A., Martin, J. A., Kinchington, D., Broadhurst, A. V., Craig, J. C., Duncan, I. B. *et al.* (1990). Rational design of peptide-based HIV proteinase inhibitors. *Science*, **248**, 358–361.
45. Krohn, A., Redshaw, S., Ritchie, J. C., Graves, B. J. & Hatada, M. H. (1991). Novel binding mode of highly potent HIV-proteinase inhibitors incorporating the (R)hydroxyethylamine isostere. *J. Med. Chem.* **34**, 3340–3342.
46. Okimoto, N., Tsukui, T., Hata, M., Hoshino, T. & Tsuda, M. (1999). Hydrolysis mechanism of the

phenylalanine-proline peptide bond specific to HIV-1 protease: investigation by the ab initio molecular orbital method. *J. Am. Chem. Soc.* **121**, 7349–7354.
47. Srinivasan, J., Cheatham, T. E. III, Kollman, P. & Case, D. A. (1998). Continuum solvent studies of the stability of DNA, RNA, and phosphoramidate-DNA helices. *J. Am. Chem. Soc.* **120**, 9401–9409.
48. Kollman, P. A., Massova, I., Reyes, C., Kuhn, B., Huo, S., Chong, L. *et al.* (2000). Calculating structures and free energies of complex molecules: combining molecular mechanics and continuum models. *Accts. Chem. Res.* **33**, 889–897.
49. Wang, W. & Kollman, P. A. (2000). Free energy calculations on dimer stability of the HIV protease using molecular dynamics and a continuum solvent model. *J. Mol. Biol.* **303**, 567–582.
50. Liang, J., Edelsbrunner, H. & Woodward, C. (1998). Anatomy of protein pockets and cavities: measurement of binding site geometry and implications for ligand design. *Protein Sci.* **7**, 1884–1897.
51. Richardson, J. S. & Richardson, D. C. (2001). MAGE, PROBE, and Kinemages, Chapter 25.2.8. In *International Tables for Crystallography* (Rossmann, M. G. & Arnold, E., eds), vol. F, pp. 727–730, Kluwer Publishers, Dordrecht.
52. Kollman, P. (1993). Free energy calculations: applications to chemical and biochemical phenomena. *Chem. Rev.* **93**, 2395–2417.
53. Massova, I. & Kollman, P. A. (2000). Combined molecular mechanical and continuum solvent approach (MM-PBSA/GBSA) to predict ligand binding. *Perspect. Drug Discovery Des.* **18**, 113–135.
54. Onufriev, A., Bashford, D. & Case, D. A. (2004). Exploring protein native states and largescale conformational changes with a modified generalized born model. *Proteins: Struct. Funct. Genet.* **55**, 383–394.

Edited by D. Case

(Received 12 February 2007; received in revised form 27 April 2007; accepted 29 April 2007)
Available online 10 May 2007

Inhibiting lentiviral replication by HEXIM1, a cellular negative regulator of the CDK9/cyclin T complex

Saki Shimizu[a,b], Emiko Urano[a], Yuko Futahashi[a], Kosuke Miyauchi[a], Maya Isogai[a], Zene Matsuda[a], Kyoko Nohtomi[a], Toshinari Onogi[a], Yutaka Takebe[a], Naoki Yamamoto[a,b] and Jun Komano[a]

Objective: Tat-dependent transcriptional elongation is crucial for the replication of HIV-1 and depends on positive transcription elongation factor b complex (P-TEFb), composed of cyclin dependent kinase 9 (CDK9) and cyclin T. Hexamethylene bisacetamide-induced protein 1 (HEXIM1) inhibits P-TEFb in cooperation with 7SK RNA, but direct evidence that this inhibition limits the replication of HIV-1 has been lacking. In the present study we examined whether the expression of FLAG-tagged HEXIM1 (HEXIM1-f) affected lentiviral replication in human T cell lines.

Methods: HEXIM1-f was introduced to five human T cell lines, relevant host for HIV-1, by murine leukemia virus vector and cells expressing HEXIM1-f were collected by fluorescence activated cell sorter. The lentiviral replication kinetics in HEXIM1-f-expressing cells was compared with that in green fluorescent protein (GFP)-expressing cells.

Results: HIV-1 and simian immunodeficiency virus replicated less efficiently in HEXIM1-f-expressing cells than in GFP-expressing cells of the five T cell lines tested. The viral revertants were not immediately selected in culture. In contrast, the replication of vaccinia virus, adenovirus, and herpes simplex virus type 1 was not limited. The quantitative PCR analyses revealed that the early phase of viral life cycle was not blocked by HEXIM1. On the other hand, *Tat*-dependent transcription in HEXIM1-f-expressing cells was substantially repressed as compared with that in GFP-expressing cells.

Conclusion: These data indicate that HEXIM1 is a host factor that negatively regulates lentiviral replication specifically. Elucidating the regulatory mechanism of HEXIM1 might lead to ways to control lentiviral replication.

AIDS 2007, **21**:575–582

Keywords: CDK9, cyclin T, HEXIM1, lentivirus, *tat*

Introduction

Activation of transcription elongation requires the positive transcription elongation factor b complex (P-TEFb) composed of cyclin dependent kinase 9 (CDK9) and cyclin T1, T2, or K [1]. P-TEFb is essential for efficient transcriptional elongation from the promoter of human immunodeficiency virus type 1 (HIV-1), the long terminal repeat (LTR) (reviewed in [2,3]). The functional interaction between P-TEFb and the viral protein Tat has been well studied. Immediately after viral transcription starts at the LTR of the integrated proviral genome, the nascent viral transcript forms a three-dimensional structure called TAR. In the presence of P-TEFb, Tat binds to TAR. Through the Tat–TAR interaction, Tat activates P-TEFb and therefore assures the efficient

From the [a]AIDS Research Center, National Institute of Infectious Diseases, Tokyo, and the [b]Department of Molecular Virology, Tokyo Medical and Dental University, Tokyo, Japan.

Correspondence to Jun Komano, AIDS Research Center, National Institute of Infectious Diseases, 1-23-1 Toyama, Shinjuku, Tokyo 162-8640, Japan.

E-mail: ajkomano@nih.go.jp

Received: 9 July 2006; revised: 25 October 2006; accepted: 13 November 2006.

ISSN 0269-9370 © 2007 Lippincott Williams & Wilkins

completion of viral gene transcription and the propagation of HIV-1.

Recently, the regulatory mechanisms of P-TEFb function have been elucidated. In 2001, the interaction of P-TEFb with 7SK RNA was found to be necessary to inactivate the kinase activity of CDK9 within P-TEFb [4–6]. However, the binding of 7SK RNA alone is not sufficient to inactivate P-TEFb. More recently, Yik *et al.* demonstrated that the inactivation of P-TEFb requires hexamethylene bisacetamide-induced protein 1 (HEXIM1; synonyms CLP1, MAQ1, and HIS1) [7–9]. The inactivation of P-TEFb by the HEXIM1-7SK RNA complex appears to regulate the transcriptional elongation of cellular genes.

The HEXIM1-7SK RNA complex has been shown to physically compete with Tat for binding to P-TEFb [10]. In agreement with this finding, HEXIM1 was shown to inhibit Tat-dependent transcription from the HIV-1 LTR in transient transfection assays [8,11,12]. However, no data demonstrating that HEXIM1 is able to limit HIV-1 replication has been provided. Here we provide direct experimental evidence that the constitutive expression of HEXIM1 specifically limits lentiviral replication.

Methods

Plasmids

The FLAG-tagged HEXIM1 expression constructs were generated by reverse-transcription PCR using RNA isolated from CEM cells as templates. The primers used were 5′-CACCTCGAGCCACCATGGACTACAAAGACGATGACGACAAGGCCGAGCCATTCTTGTC-3′ and 5′-CAATTGCTAGTCTCCAAACTTGGAAAGCGGCGC-3′′ for amino terminus FLAG tagging, and 5′-CACCTCGAGCCACCATGGCCGAGCCATTCTTGTCAGAATATC-3′ and 5′-CAATTGCTAGTCGTCATCGTCTTTGTAGTCGTCTCCAAACTTGGAAAGCGGCGCTC-3′ for carboxy terminus FLAG tagging. The *Xho*I-*Mfe*I fragments of the PCR products were cloned into the *Xho*I-*Mfe*I sites of pCMMP IRES GFP, generating pCMMP f-HEXIM1 and pCMMP HEXIM1-f [13]. The cytomegalovirus (CMV) promoter-driven *gag-pol* expression vector psyn*gag-pol* has been previously described by Wagner *et al.* [14] and pLTR*gag-pol* was constructed by cloning the *Mlu*I-*Hin*dIII fragment encoding the LTR from pNL-luc [15] into the *Mlu*I-*Hin*dIII sites of psyn*gag-pol*. The tax expressing plasmid pCGtax and pHTLV LTR luciferase were kindly provided by Dr. Watanabe (Tokyo Medical Institute). The *tat*-expressing plasmid pSVtat was a generous gift from Dr. Freed (National Cancer Institute-Frederick, Frederick, Maryland, USA). The plasmid pLTR-luc has been described previously (Miyauchi *et al.*, *Antiviral Chemistry and Chemotherapy*, in press). The following plasmids have been described previously by Komano *et al.* [13]: pVSV-G, pMD*gag-pol*, pTM3Luci, phRL-CMV and pSIVmac239ΔnefLuc.

Cells and transfection

All the mammalian cells were maintained in RPMI 1640 (Sigma, St Louis, Missouri, USA) supplemented with 10% fetal bovine serum (Japan Bioserum, Tokyo, Japan), penicillin and streptomycin (Invitrogen, Tokyo, Japan). Cells were incubated at 37°C in a humidified 5% CO_2 atmosphere. Cells were transfected using Lipofectamine 2000 according to the manufacturer's protocol (Invitrogen).

Western blotting

Cells were lysed with sample buffer, sonicated, and boiled for 5 min. Samples were separated on 8% sodium dodecyl sulfate-polyacrylamide gel electrophoresis gels and transferred to polyvinylidene difluoride membranes (Millipore, Billerica, Massachusetts, USA) for western blotting according to standard techniques. Membranes were blocked with Tris-buffered saline containing 0.05% Tween-20 (TBS-T) containing 5% (w/v) non-fat skim milk (Yuki-Jirushi, Tokyo, Japan) for 1 h at room temperature and incubated with primary antibodies including the M2 anti-FLAG epitope monoclonal antibody (Sigma), an anti-actin monoclonal antibody (MAB1501R; Chemicon/Millipore, Billerica, Massachusetts, USA), an anti-cyclin T1 rabbit polyclonal antibody (H-245; Santa Cruz Biotechnology, Santa Cruz, California, USA), an anti-cyclin T2a/b goat polyclonal antibody (A-20; Santa Cruz), an anti-p24 monoclonal antibody (183-H12-5C; NIH AIDS Research and Reference Reagent Program), an anti-HIS1 chicken polyclonal antibody (N-150; GenWay, San Diego, California, USA), and an anti-Bip/GRP78 monoclonal antibody (clone 40; BD Biosciences/Transduction Laboratories, San Jose, California, USA) for 1 h at room temperature. Membranes were washed with TBS-T and incubated with appropriate second antibodies including biotinylated anti-goat (GE Healthcare Bio-Sciences, Piscataway, New Jersey, USA) or anti-chicken IgY (Promega, Madison, Wisconsin, USA), and EnVision+ (Dako, Glostrup, Denmark) for 1 h at room temperature. For a tertiary probe, we used horseradish peroxidase (HRP)-streptavidine (GE Healthcare) if necessary. Signals were visualized with an LAS3000 imager (Fujifilm, Tokyo, Japan) after treating the membranes with the Lumi-Light Western Blotting Substrate (Roche Diagnostics GmbH, Mannheim, Germany).

Reporter assay

Luciferase activity was measured 48 h after transfection or infection using a DualGlo assay kit (Promega) according to the manufacturer's protocol. The beta-galactosidase activity was measured using a LumiGal assay kit (BD Biosciences/Clontech, San Jose, California, USA) according to the manufacturer's protocol. The

chemiluminescence was detected with a Veritas luminometer (Promega).

Monitoring viral replication

To monitor HIV-1 replication, the culture supernantants were subjected to either a reverse transcriptase assay [16] or an enzyme-linked immunosorbent assay (ELISA) to detect p24 antigens using a Retro TEK p24 antigen ELISA kit according to the manufacturer's protocol (Zepto Metrix, Buffalo, New York, USA). For simian immunodeficiency virus (SIV) a p27 antigen ELISA kit was used according to the manufacturer's protocol (Zepto Metrix). The signals were measured with a Multiskan Ex microplate photometer (ThermoLabsystems, Helsinki, Finland). For vaccinia virus, adenovirus, and herpes simplex virus (HSV)-1, the activity of reporter genes was measured as previously described [13].

Generating viruses

To produce HIV-1 and SIV, 293T cells were transfected with plasmids encoding proviral DNA of HIV-1 (pHXB2) or pSIVmac239ΔnefLuc and culture supernatants containing viruses were collected at 48 h post-transfection. Murine leukemia virus (MLV) and lentiviral vectors pseudotyped with VSV-G were produced as described previously by cotransfecting 293T cells with either the pNL-Luc and pVSV-G vectors or the pMD*gag-pol*, pVSV-G, and pCMMP vectors [13]. Green fluorescent cells were sorted by fluorescence activated cell sorter (FACS) Aria (Becton Dickinson, San Jose, California, USA).

Reverse transcriptase-polymerase chain reaction

Total RNA was isolated with an RNeasy kit (Qiagen GmbH, Hilden, Germany) according to the manufacturer's instruction. The reverse transcriptase (RT)-polymerase chain reaction (PCR) assay was performed with a One Step RNA PCR Kit (Takara, Otsu, Japan), imaged by a Typhoon scanner 9400 (GE Healthcare), and quantified with Image Quant software (GE Healthcare). For the amplification of endogenous HEXIM1, the forward primer 5′-ACCACACGGAGAGCCTGCAGAAC-3′ and the reverse primer 5′-TAGCTAAATTTACGAAACCAAAGCC-3′ were used. For the amplification of HEXIM1-f, the forward primer 5′-GTACCTGGAACTGGAGAAGTGCCC-3′ and the reverse primer 5′-CAATTGCTAGTCGTCATCGTCTTTGTAGTC-3′ were used. For cyclophilin A, the forward primer 5′-CACCGCCACCATGGTCAACCCCACCGTGTTCTTCGAC-3′ and the reverse primer 5′-CCCGGGCCTCGAGCTTTCGAGTTGTCCACAGTCAGCAATGG-3′ were used.

Quantitative real time polymerase chain reaction

The real time PCR reaction was performed in a DNA Engine Opticon 2 Continuous Fluorescence Detection System (Bio-Rad, Hercules, California, USA). The cellular genomic DNA and total RNA were extracted 48 h post-infection with a DNeasy kit (Qiagen) and RNeasy kit (Qiagen), respectively, according to the manufacturer's instruction. For the reagents, we used QuantiTect SYBR Green PCR and RT-PCR Kits (Qiagen). To estimate the amount of integrated HIV-1 DNA, Alu-LTR PCR was performed according to the method described previously using the following primers: for the first PCR, 5′-AACTAGGGAACCCACTGCTTAAG-3′ and 5′-TGCTGGGATTACAGGCGTGAG-3′, and for the second PCR, 5′-AACTAGGGAACCCACTGCTTAAG-3′ and 5′-CTGCTAGAGATTTTCCACACTGAC-3′ [17]. The beta-globin primers have been described previously [18]. To estimate the amount of HIV-1 RNA, the second PCR primers for the Alu-LTR PCR were used. The primers for cyclophilin A are described above.

Results and discussion

The HEXIM1 cDNA tagged with a FLAG epitope at either the amino terminus (f-HEXIM1) or the carboxy terminus (HEXIM1-f) was cloned in a mammalian expression plasmid (Fig. 1a). A luciferase assay revealed that the Tat-dependent enhancement of transcription from the HIV-1 LTR was reduced by co-transfecting HEXIM1-expressing plasmids, whereas neither Tat-independent basal transcription from the HIV-1 LTR nor CMV promoter-driven transcription was affected (Fig. 1b). An oncogenic retrovirus human T cell leukemia virus type 1 (HTLV-1) encodes for *tax*, a functional homologue of HIV-1's *tat*, that utilizes P-TEFb to enhance transcription from the LTR promoter [19]. However, *tax*-dependent enhancement of transcription was not affected by HEXIM1 in similar experimental conditions (Fig. 1c). To monitor the effect of HEXIM1 on HIV-1 replication, we introduced HEXIM1-expressing plasmids into HeLa-CD4 cells along with pNL4-3, which produces replication-competent HIV-1, and measured the RT activity in the culture supernatant 1 week post-transfection. Transfecting HEXIM1-expressing plasmids decreased the RT activity in a dose-dependent manner (Fig. 1d). Next, we asked whether the inhibition of viral replication was specific to HIV-1 by examining vaccinia virus, adenovirus, and HSV-1 replication. We found that the propagation of these three viruses was not inhibited by HEXIM1-f expression (Fig. 1e–g), suggesting that the inhibition of viral replication by HEXIM1 was HIV-1-specific.

To examine whether HEXIM1 negatively affects lentiviral replication in the physiologically relevant host, we isolated human T cell lines constitutively expressing HEXIM1-f. We cloned HEXIM1-f cDNA into a pCMMP (MLV retroviral vector plasmid (Fig. 2a). The plasmid encoded an internal ribosomal entry site (IRES)-mediated green fluorescent protein (GFP) expression cassette, so that MLV vector-infected cells

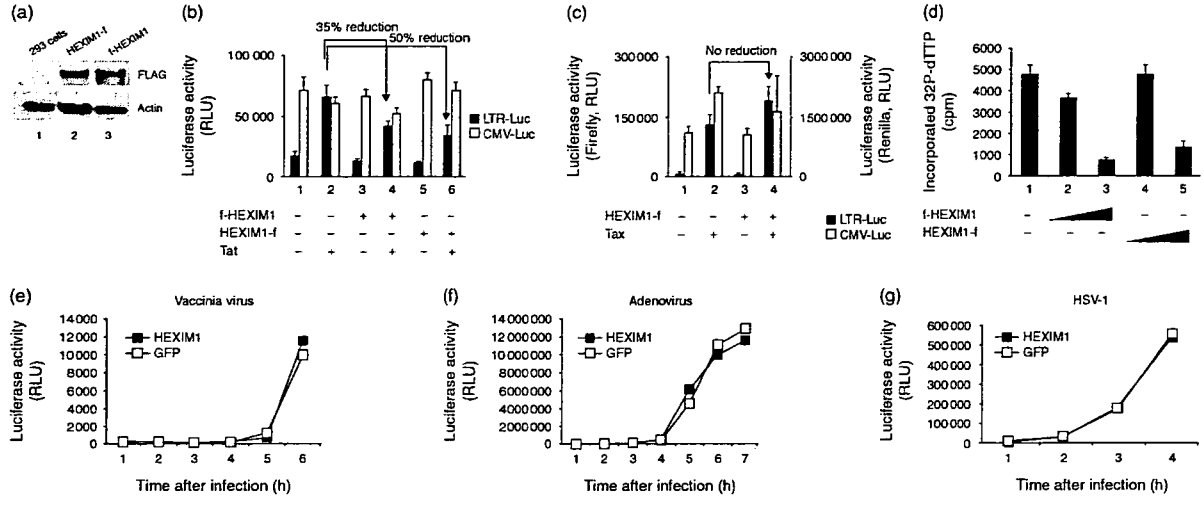

Fig. 1. Expression of hexamethylene bisacetamide-induced protein 1 (HEXIM1) specifically inhibits HIV-1 replication. (a) Detection of HEXIM1 cDNA tagged with a FLAG epitope at either the amino terminus (f-HEXIM1) or the carboxy terminus (HEXIM1-f) by western blot analysis in transiently transfected 293 cells (upper panel, approximately 65 kD). A western blot against actin is shown as a loading control (lower panel). (b) Expressing FLAG-tagged HEXIM1 decreased the luciferase activity driven by HIV-1 long terminal repeat (LTR) promoter in the presence of Tat (lanes 4 and 6, LTR-Luc, solid bars). However, FLAG-tagged HEXIM1 did not affect the expression of renilla luciferase from co-transfected plasmid driven by the cytomegalovirus (CMV) promoter (CMV-Luc, open bars). Representative data from three independent experiments done in triplicate are shown. Cells were transfected with 0.8 μg HEXIM1-expressing plasmid for the indicated lanes, 0.1 μg of pSV*tat* for the indicated lanes, and 0.1 μg of pLTR-Luc and 0.5 μg for phRL/CMV for all lanes. (c) Expressing FLAG-tagged HEXIM1 did not decrease the luciferase activity driven by HTLV-1 LTR promoter in the presence of Tax (lanes 2 and 4, LTR-Luc, solid bars) as well as renilla luciferase driven by the CMV promoter (CMV-Luc, open bars). Representative data from three independent experiments done in triplicate are shown. Cells were transfected with 0.8 μg of HEXIM1-expressing plasmid for the indicated lanes, 0.1 μg of pCGtax for the indicated lanes, and 0.1 μg of pHTLV LTR Luc and 0.5 μg for phRL/CMV for all lanes. (d) The dose-dependent reduction of HIV-1 production by transfection of HEXIM1-encoding plasmids (0.1 μg for lanes 2 and 4, 0.4 μg for lanes 3 and 5) along with a plasmid producing infectious HIV-1 (pNL4-3, 0.1 μg) in HeLa-CD4 cells. (e–g) Expressing HEXIM1-f did not limit the replication of vaccinia virus (e), adenovirus (f), or HSV-1 (g) in 293T cells. The *y*-axis represents the reporter gene activity, which reflects viral replication. Representative data from three independent experiments are shown. GFP, green fluorescent protein; RLU, relative light unit.

could be readily identified by the green fluorescence. Human T cell lines, including SUP-T1, MOLT-4, CEM, Jurkat, and M8166 were infected with MLV pseudotyped with vesicular stomatitis virus glycoprotein (VSV-G), and GFP-positive cells were collected with a FACS (Fig. 2a). For the negative control, we used MLV expressing GFP only. The successful introduction of HEXIM1-f into the cells was verified by RT-PCR and Western blot analysis (Fig. 2b and c). The total HEXIM1 protein expression in HEXIM1-f-transduced cells was approximately 3.7-, 1.5-, 2.0-, 4.8-, and 1.8-fold higher than in GFP-transduced cells in the CEM, Jurkat, MOLT-4, SUP-T1, and M8166 cell lines, respectively (Fig. 2c). To our surprise, the HEXIM1-f-expressing T cell lines remained GFP-positive, and therefore HEXIM1-f-positive, for more than 6 months and proliferated at rates almost indistinguishable from GFP-expressing cells. The expression levels of cyclin T1, cyclin T2, actin, and Bip/GRK78 in HEXIM1-f-expressing cells were almost identical to those in GFP-expressing cells, suggesting that the gene expression did not compensate the upregulated HEXIM1 (Fig. 2b and c). Expression of cyclin T2 was undetectable in M8166 cells (Fig. 2c). Similarly, HEXIM1-f expression did not affect the cell surface levels of the HIV-1 receptors CD4 and CXCR4 as demonstrated by FACS analysis (data not shown). These data indicate that the expression of HEXIM1-f did not reach levels where the physiological regulation of P-TEFb blocked cellular gene transcription.

The replication kinetics of HIV-1 or SIV was monitored by measuring the accumulation of viral capsid antigen in the culture medium. Strikingly, HIV-1 replicated more slowly in cells of all four T cell lines expressing HEXIM1-f than in cells expressing GFP (Fig. 2d–g). Similarly, HEXIM1-f-expressing M8166 cells supported SIV replication less efficiently than did GFP-expressing M8166 cells (Fig. 2h). Interestingly, the magnitude of HIV-1 replication delay was the most substantial in SUP-T1 cells, in which the levels of endogenous HEXIM1 were the lowest among the four cell lines tested for HIV-1 replication (Fig. 2c). Similar observations were made when the HIV-1 infection experiments were repeated, indicating that the expression of functional HEXIM1-f did not change over the course of the replication monitoring. We tested whether the viruses emerged in

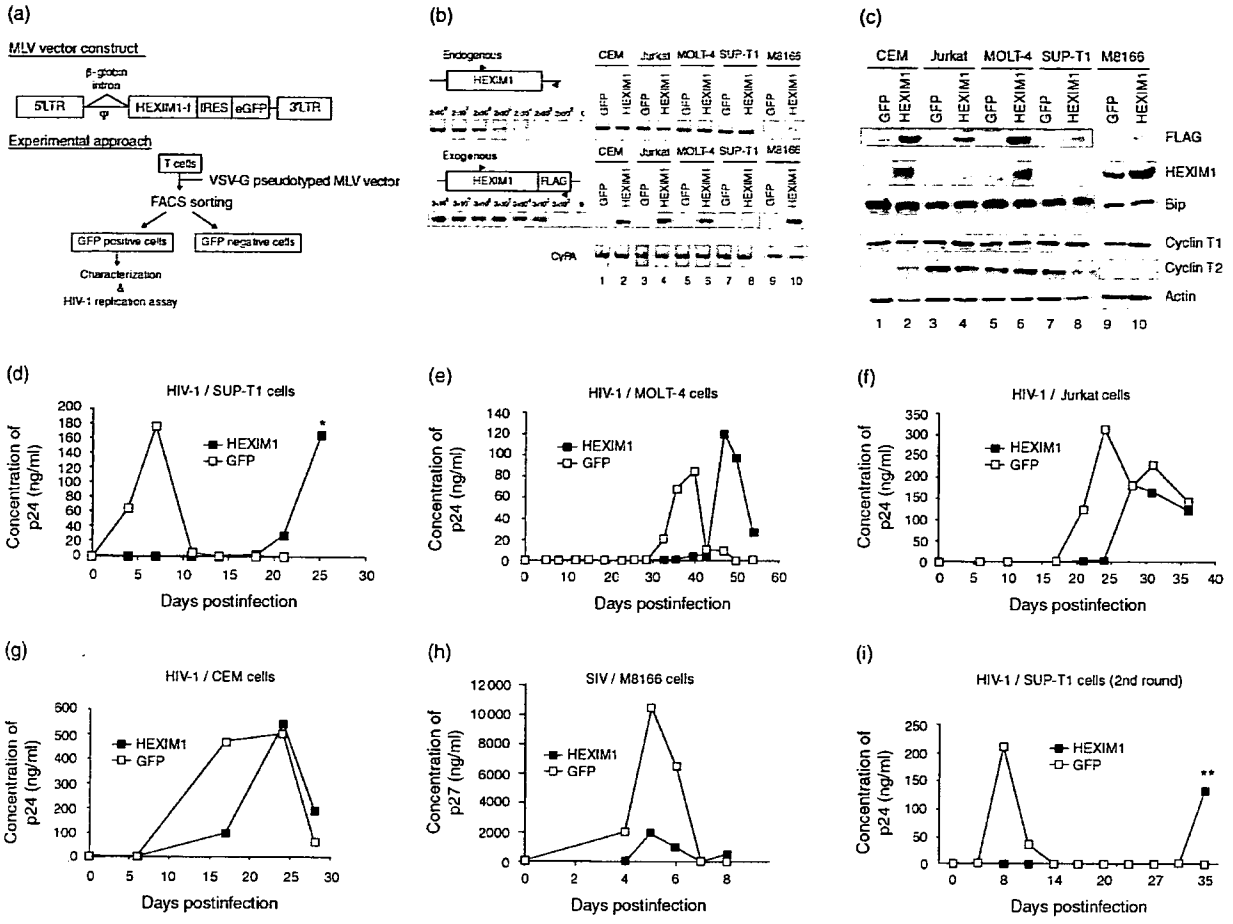

Fig. 2. Lentiviral replication is inhibited in various T cell lines constitutively expressing hexamethylene bisacetamide-induced protein 1 (HEXIM-1) cDNA tagged with a FLAG epitope at the carboxy terminus (HEXIM1-f). (a) The genomic organization of the retroviral vector expressing HEXIM1-f and a schematic representation of the experimental approach. (b) Detection of endogenous HEXIM1 and murine leukemia virus (MLV)-transduced HEXIM1-f (exogenous) mRNA by reverse transcriptase-polymerase chain reaction in green fluorescent protein (GFP)- and HEXIM1-f-expressing cells. The primer design is drawn schematically. Amplification efficiency was examined by using a known number of templates as standards for HEXIM1. Cyclophilin A (CyPA) was amplified to ensure the quality of the RNA. (c) Western blot analysis demonstrating expression of HEXIM1-f (denoted FLAG), endogenous HEXIM1 (HEXIM1), Bip, cyclin T1, cyclin T2, and actin in isolated T cell lines. (d–g) Replication profiles of HIV-1 (HXB2) in SUP-T1 (d), MOLT-4 (e), Jurkat (f), and CEM (g) cells either expressing HEXIM1-f or GFP alone. Representative data from two or three independent experiments are shown. (h) Replication profile of SIV in M8166 cells either expressing HEXIM1-f or GFP alone. Representative data from two independent experiments are shown. (i) The replication profiles of HIV-1 recovered from SUP-T1/HEXIM1-f cells (asterisk in Fig. 2d) in fresh SUP-T1/GFP or SUP-T1/HEXIM1-f. LTR, long terminal repeat.

HEXIM1-f-expressing cells were 'revertants' that might be able to replicate in HEXIM1-f-expressing cells as fast as in GFP-expressing cells. To address this, we recovered virus-containing culture supernatants from SUP-T1/HEXIM1-f cells at the peak of replication kinetics (asterisk, Fig. 2d). Then, both fresh SUP-T1/GFP and SUP-T1/HEXIM1-f were infected with the recovered virus and the replication kinetics was monitored. However, HIV-1 still replicated in SUP-T1/HEXIM1-f cells more slowly than in SUP-T1/GFP cells (Fig. 2i), akin to the original profiles (Fig. 2d), and the nucleotide sequences of LTR and *tat*, the primary targets of HEXIM1, remained unchanged (double asterisk in Fig. 2i). In addition, no mutations were found in viruses propagated in GFP-expressing SUP-T1 cells. Similar observations were made in MOLT-4 cells (data not shown). These data provide direct evidence that the expression of HEXIM1 inhibits lentiviral replication in human T cell lines.

Based on our experimental observations as well as the reported functions of HEXIM1, we assumed that the ability of HEXIM1 to limit HIV-1 replication was mostly due to the inhibition of Tat/P-TEFb-dependent transcriptional elongation. However, it was possible that HEXIM1 might also have targeted other viral replication

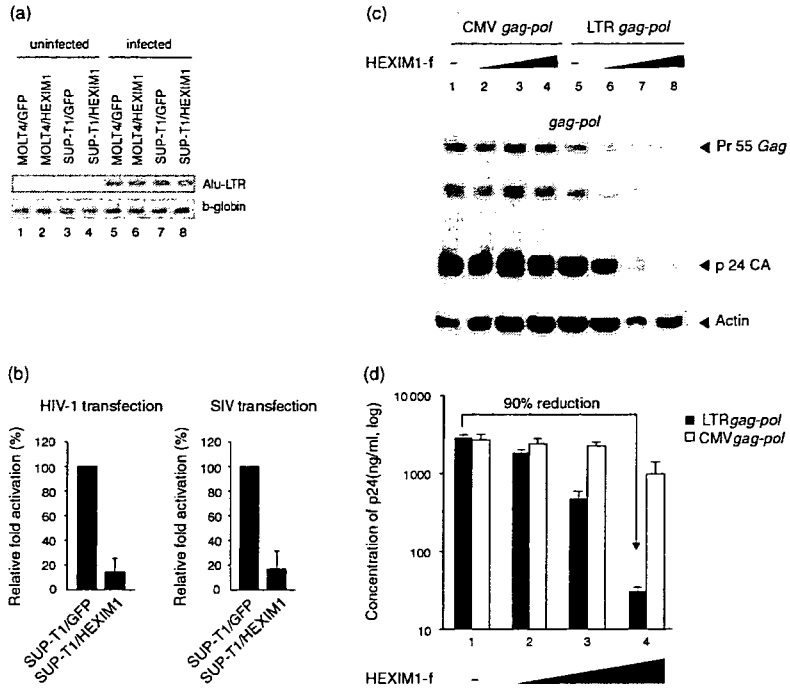

Fig. 3. Hexamethylene bisacetamide-induced protein 1 (HEXIM1) cDNA tagged with a FLAG epitope at the carboxy terminus (HEXIM1-f) does not affect the efficiency of viral integration or post-translational processes. (a) The Alu-long terminal repeat (LTR) and beta-globin polymerase chain reaction products from VSV-G-pseudotyped HIV-1-infected MOLT-4 and SUP-T1 cells expressing either green fluorescent protein (GFP) or HEXIM1-f alone were separated in an agarose gel and photographed. (b) The luciferase activities in SUP-T1/GFP or SUP-T1/HEXIM1-f cells electroporated with 10 μg of a plasmid encoding LTR-driven firefly luciferase plus 1 μg of phRL/cytomegalovirus (CMV). The firefly luciferase activity normalized to renilla luciferase activity in SUP-T1/GFP cells was set to 100%. The error bars represent the standard deviation of three independent experiments. (c) Western blot analysis showing Gag and its cleaved products expressed from either CMV promoter- or LTR promoter-driven *gag-pol* expression plasmid in the presence of pSVtat (0.1 μg, all lanes) and increasing amounts of HEXIM1-f (0.2 μg for lanes 2 and 6, 0.6 μg for lanes 3 and 7, and 2.0 μg for lanes 4 and 8). (d) The amount of p24 produced in the culture supernatant from cells analyzed in Fig. 3c was measured by enzyme-linked immunosorbent assay. Representative data from three independent experiments done in triplicate are shown. SIV, simian immunodeficiency virus.

steps. To test this possibility, we examined the viral entry and production processes separately. The efficiency of viral entry was analyzed by measuring the efficiency of viral integration. SUP-T1/GFP or SUP-T1/HEXIM1-f cells were infected with a replication-incompetent HIV-1 vector pseudotyped with VSV-G that expresses luciferase upon successful infection. We conducted an Alu-LTR PCR assay to detect the integrated viral genome. PCR products were detected only from HIV-1-infected cells (Fig. 3a). The signal intensities of Alu-LTR PCR products from GFP- and HEXIM1-f-experssing cells were similar. To compare the efficiency of viral infection as well as transcription quantitatively, we employed a real time PCR technique. Some infected cells were collected for an Alu-LTR PCR assay to quantify the amount of integrated viral genome, and the rest were processed to measure the amount of viral transcript as well as the luciferase activity. The amount of Alu-LTR PCR product from SUP-T1/HEXIM1-f cells was 3.5- and 3.3-fold more to that from SUP-T1/GFP cells from two independent experiments, respectively (Table 1). These data suggest that the efficiency of viral integration was not inhibited in HEXIM1-f-expressing SUP-T1 cells. In contrast, the relative abundance of HIV-1 transcript expressed in SUP-T1/HEXIM1-f cells was substantially decreased to 0.03 and 2.9% relative to SUPT1/GFP cells (Table 1). Furthermore, the luciferase activities were 200-fold lower in SUP-T1/HEXIM1-f cells than in SUP-T1/GFP cells (Table 1). Similar data was obtained from MOLT-4 cells infected with HIV-1 pseudotyped with VSV-G (data not shown). The transfection of plasmids encoding reporter viral DNA can bypass the viral entry and make it possible to measure the effect of HEXIM1 on LTR-driven transcription and translation. Consistent with above data, transfecting pNL-Luc into SUP-T1/HEXIM1-f cells gave significantly lower luciferase activities than SUP-T1/GFP cells (Fig. 3b, left). Similar data were obtained using pSIVmac239ΔnefLuc (Fig. 3b, right). These data strengthen the possibility that HEXIM1 targets post-integration processes.